Universität Bremen

AWI Alfred-Wegener-Institut für Polar- und Meeresforschung in der Helmholtz-Gemeinschaft

Master's Thesis

Modelling mid-Pliocene climate with COSMOS based on PlioMIP2 boundary conditions

Author:

Eric Kayode Samakinwa

Matriculation Number:

3031466

Examiners:

Prof. Dr. Gerrit Lohmann

Dr. Christoph Völker

Supervisor:

Dr. Christian Stepanek

Submitted

to

Institute of Environmental Physics (IUP),

University of Bremen, Bremen, Germany

July 3, 2018

in partial fulfillment of the requirements for the award of master of science (M.Sc) in Environmental Physics.

Declaration of copyright

I hereby declare, that this master thesis was written without external support and that sources and auxilliary means other than those quoted in this report were not used. All statements which were literally or analogously taken from other publications have been identified as quotations.
Furthermore, I authorize this study to be made available on the research archive webpage of the Postgraduate Program ENVIRONMENTAL PHYSICS (PEP), University of Bremen, Germany.

Bremen / July 3, 2018. **Eric Kayode Samakinwa**

List of Figures

List of Tables

Abstract

The mid-Pliocene warm period has been suggested as an analog to a future warmer climate (Jansen et al., 2007), due to its similarity to present day in terms of land-sea distribution as well as CO_2. The Pliocene Model Intercomparison Project (PlioMIP), established by Haywood et al. (2010, 2011), is an internationally coordinated effort to identify strengths and weaknesses of climate models in simulating of mid-Pliocene climate. PlioMIP is currently in its second phase, due to advances in the understanding of palaeogeography, ocean, terrestrial and cryosphere of the Pliocene epoch. Boundary conditions have been updated from PlioMIP1 and experiments were prescribed accordingly for PlioMIP2. In this study, a detailed description of the different components of the utilized Community Earth System Models (COSMOS, version: COSMOS-landveg r2413, 2009) as well as experimental procedures prescribed for PlioMIP2 (Haywood et al., 2016) are provided. Furthermore, the procedures applied to transfer the Pliocene Research, Interpretation and Synoptic Mapping (PRISM) Project mid-Pliocene reconstruction into model forcing is documented.

The mid-Pliocene, as simulated by COSMOS and the PlioMIP2 prescribed boundary conditions is warmer than the PI-control simulation by 2.15 K in the global mean, corresponding to 0.08 K colder than the PlioMIP1 simulation by the same model. Higher-latitude warming, which is supported by the proxy evidences is still underestimated in the model outputs. The state of the Bering Strait, which is unknown during the mid-Pliocene

(Gladenkov et al., 2002) was opened for PlioMIP1 and closed for PlioMIP2 simulations. This study show that a closed Bering Strait leads to better agreement of COSMOS simulations with SST reconstruction in North Atlantic. Data-model discrepancies are not fully resolved even with the closure of the Bering Strait, this study show that uncertainty in the concentration of atmospheric CO_2 contributes to the disagreement in various Ocean regions.

Furthermore, climate sensitivity is estimated for climate states with two different background geographies, and the results confirmed that the response of global temperature to the doubling of CO_2 is dependent on the background climate.

Contents

CHAPTER 1

Introduction

Human population has increased by atleast 1.3% per year since 1998, and could be doubled by the end of 2050 (UNESCO , 2010). The direct implication of this on the climate system include increased concentration of atmospheric CO_2 through anthropogenic activities, increased energy demand in some part of the world hampering the urban microclimate of these locations, loss of polar seaice and a combined effect increasing global temperatures. Through the continuous release of long-lived gases such as CO_2 in the atmosphere, future warming is almost inevitable. It is however important to have a feel of what the climatic condition in the nearest future would look like, to enable proper mitigation measures. The mid-Pliocene (3.29 - 2.97 Ma BP) has been suggested as the time-slice which could provide a possible insight to future climate, in terms of warming (Jansen et al. , 2007). Climate model simulations of this time-slice has reported global mean temperatures which are 2 - 3 degrees higher that of the present-day (Haywood and Valdes, 2004; Jansen et al. , 2007), thus the mid-Pliocene can be a useful but not direct analogue for future warmth.

The Pliocene epoch, refer to the uppermost subdivision of the Cenozoic era (since about 66 million years (Ma) before Present (BP)) before the Quaternary (2.58 Ma to 0 Ma BP). It covers a time frame from ca 5.33 to 2.58 Ma BP, according to the geological time

scale of Walker et al. (2013). The Pliocene is sub-divided into Piacenzian and Zanclean ages. The mid-Piacenzian Warm Period is a relatively short warm period which spans from about 3.29 to 2.97 Ma BP (Lunt et al., 2010). The mid-Pliocene climate can be inferred into through records of past climate stored in geological archives, and by forcing climate models with boundary conditions that are near-perfect representative of the time-slice. In most studies, climate model outputs are compared with geological proxy data to check their level of agreement. Climate models utilize boundary conditions to represent the altered configuration of land surface, ocean bathymetry as well as the atmospheric compositions and orbital configuration representative of the time-slice under study. Furthermore, derivation of vegetation distribution may be necessary if such is not modelled itself. Creating boundary conditions for past time periods is one of the most time consuming tasks faced in palaeoclimate modelling. Assumptions with respect to palaeoclimate boundary conditions can vary amongst researchers, and the mid-Pliocene is not an exceptional time-slice in this respect. Therefore, to provide common grounds for the model intercomparison in simulating the mid-Pliocene Warm Period (mPWP), the Pliocene Modelling Intercomparison Project (PlioMIP) provide sets of boundary conditions that is implemented consistently across ensemble models.

PlioMIP works in alliance with the US Geological Survey's Pliocene Research Interpretation and Synoptic Mapping (PRISM) project (Dowsett et al., 2013). Different sets of geological reconstructions of the mid-Pliocene were produced since the early 1990s, the first version named PRISM0 was presented by Dowsett et al. (1994). PRISM1, PRISM2, PRISM3D and PRISM4 were presented as updates to the initial reconstruction effort in 1996, 1999, 2007 and 2016, respectively (Dowsett et al., 2013). The PRISM project provides this data in form of gridded boundary condition data suitable for use in GCMs. PlioMIP is already in its second phase, phase 1 (PlioMIP1) having been wrapped up in 2015. Since its inception in 2008, it has identified consistency among models in simulating surface air in the tropics, a lack of model consistency in the simulated temperature response at high latitudes, and inconsistency in model predictions of the total precipitation rate in the tropics (Haywood et al., 2010). Furthermore, there is no clear indication in PlioMIP1 model ensemble to support either enhanced or weakened Atlantic Meridional Overturning Circulation (AMOC) and related ocean heat transport to the high latitudes,

as model simulations show enhanced as well as reduced AMOC and ocean heat transport to high latitudes of various amplitudes (Zhang et al., 2013). PlioMIP1 demonstrated the requirement to better understand boundary condition uncertainties as well as weaknesses in the methodologies used for datamodel comparison, which largely arise from the time-averaged nature of proxy data used in previous datamodel comparisons (Dowsett et al., 2013; Salzmann et al., 2013). Inference from model results indicates that longer-term climate sensitivity (Earth system sensitivity (ESS)) is greater than Charney's sensitivity (best estimate ESS/CS ratio of 1.5; (Haywood et al., 2013)).

Following the conclusion of phase 1, Phase 2 will utilize state-of-the-art boundary conditions that have emerged over the last 5 years including new palaeogeography reconstruction detailing ocean bathymetry and landice surface topography as well as new data sets describing the distribution of Pliocene soils and lakes. The ice surface topography is built upon the Pliocene Ice Sheet Model Intercomparison Project (PLISMIP) (Dolan et al., 2015) that was a spin-off of PlioMIP1 and is based on simulated climate data from ice sheet distribution and extent based on climate forcing produced by PlioMIP1 model ensemble. Reconstruction of atmospheric-CO_2 are emerging on orbital timescales (Badger et al., 2013; Bartoli et al., 2011) and land surface cover details will be enhanced by recent additions of Pliocene soils and lakes (Pound et al., 2014). All these improved dataset of boundary conditions are incorporated into PlioMIP2. Based on these new datasets, further modelling studies will be conducted in PlioMIP2 to increase the understanding of temporal changes in Pliocene climate. This would be done by generating new data through multi-proxy methods which will focus on key locations that have been identied by PlioMIP1 as important for understanding Pliocene climate variability (Haywood et al., 2016).

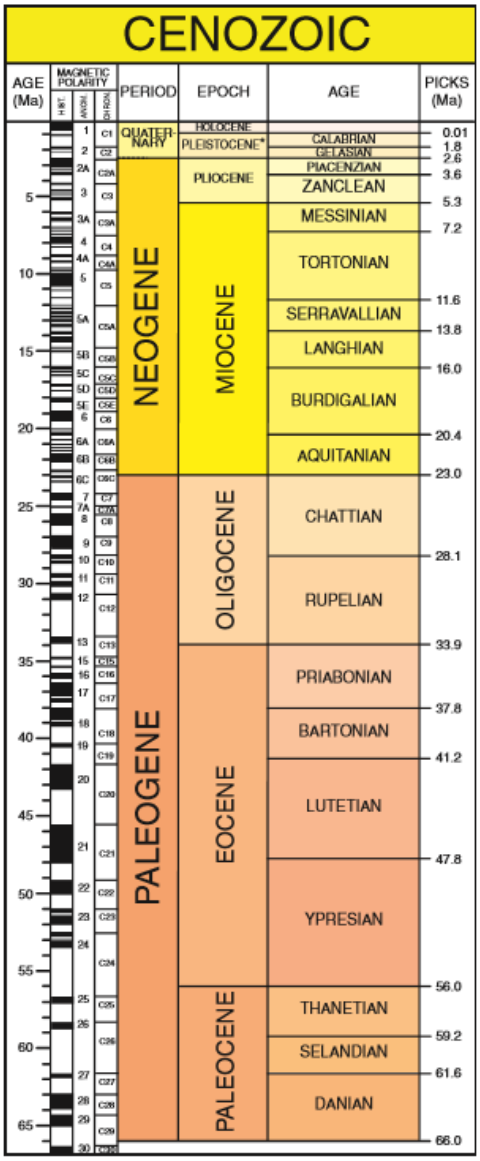

Figure 1.1: Geological timescale showing the Cenozoic era, modified from Walker et al. (2013).

1.1 Working hypotheses

1.1.1 Hypothesis 1: Climate sensitivity is dependent on the background climate and on the state of the imposed boundary conditions

Climate sensitivity (CS) is a term used to describe the response of the climate system to an imposed radiative forcing. It is commonly defined within the climate modelling community as the equilibrium global mean surface temperature change that occurs in response to a doubling of atmospheric CO_2 concentration from the PI value (Chylek and Lohmann, 2008).

Several studies have suggested different climate sensitivity (CS) estimates, and also presented arguments about different CS for cold and warm climates. Knutti et al. (2006)

Table 1.1: Climate sensitivity of PlioMIP1 ensemble models (Hargreaves and Annan, 2016; Haywood et al., 2013)

Model	Reference	CS (K)
COSMOS	Stepanek and Lohmann (2012)	4.1
CCSM4	Rosenbloom et al. (2013)	3.2
FGOALS-g2	Zheng et al. (2013)	3.7
GISS ModelE2-R	Chandler et al. (2013)	2.8
HadCM3	Bragg et al. (2012)	3.1
IPSLCM5A	Contoux et al. (2012)	3.4
MIROC4m	Chan et al. (2011)	4.05
MRI-CGCM2.3	Kamae and Ueda (2012)	3.2
NorESM-L	Zhang et al. (2012)	3.1

reported that CS is very unlikely (5 % probability) to be either below 1.5-2 K or above about 5-6.5 K, with the best agreement found for values between 3 and 3.5 K. Friedrich et al. (2016) conclude that warm climates are more sensitive to changes in CO_2 levels than cold climates. In the framework of PlioMIP1, a CS of 4.1 K was obtained for the doubling of CO_2 with respect to COSMOS simulations (Haywood et al., 2013). Other PlioMIP model ensembles gave different values of CS as shown in Table 1. A methodology is proposed in the framework of PlioMIP2 to further investigate the dependence of CS on the background climate and the imposed boundary conditions (Haywood et al.,

2016). For the COSMOS, the dependency of CS on the underlying climate is investigated with two different background climates. Representatives of mid-Pliocene and the pre-industrial climates are utilized in this respect. The analysis and results are presented in chapter 4.

1.1.2 Hypothesis 2: Agreement between simulated North Atlantic SSTs with reconstruction of the mid-Pliocene is better if the Bering Strait is closed

Analysing proxy-reconstructed paleoclimate records and models in tandem allows the evaluation of climate transitions through the analysis of forcing and feedback mechanisms in past and future climate changes (Lohmann et al., 2008). Sea surface temperature (SST) as simulated by COSMOS in the framework of PlioMIP1, show regionally a weak agreement with the reconstruction. PlioMIP1 model ensembles show a persistent underestimation of the reconstructed North Atlantic Ocean SST (Dowsett et al., 2013). Furthermore, climate model simulations have been unable to achieve the high-latitude warming estimated for both terrestrial and marine environments of the mid-Pliocene (Dowsett et al., 2013; Salzmann et al., 2013).

Furthermore, the effect of a closed Bering Strait in paleoclimate simulations has been shown to increase Atlantic Meridional Overturning Circulation (AMOC), which provides an increased ocean heat transport to the North Atlantic (Hu et al., 2015). Freshwater transport from the Pacific to the Arctic Ocean and from the Arctic Ocean to the Labrador Sea, leads to warmer sea surface temperatures in the North Atlantic (Otto-Bliesner et al., 2017). Hu et al. (2015) show that, regardless of the climate state, a closed Bering Strait produces a warmer North Atlantic. Thus, a closed Bering Strait in PlioMIP2 (that was assumed to be open in PlioMIP1) may improve the fit between existing mid-Pliocene marine and terrestrial data and model simulations (Dowsett et al., 2016). With the new PlioMIP2 state-of-the-art boundary conditions, this study further investigates the effect of a closed Bering Strait in achieving a better agreement between simulated mid-Pliocene SSTs and the reconstruction.

1.1.3 Hypothesis 3: Uncertainty in CO_2 concentration can account for high and low latitude data-model mismatches.

Sensitivity tests of PlioMIP ensemble models reported by Salzmann et al. (2013), identified insufficient temporal constraints hampering the accurate configuration of model boundary conditions as an important factor impacting on data-model discrepancies. It was concluded that a more defined orbital time slice will allow a robust evaluation of present climate models to predict warm climates. SSTs as simulated by COSMOS in the framework of PlioMIP1, show regionally a weak agreement with the reconstruction. According to the result presented by Stepanek and Lohmann (2012) for COSMOS simulations in PlioMIP1, SSTs of the mid-Pliocene simulation show that the equatorial warm pool of the Atlantic Ocean, the Pacific Ocean, and the Indian Ocean are characterized by increased maximum temperature and spatial extent. Such warming is not in agreement with the reconstruction. In the framework of PlioMIP2, a more defined orbital time slice (KM5c Marine Isotope Stage) has been specified (Haywood et al., 2016). This study will evaluate the effect of CO_2 uncertainty in achieving a reasonable agreement between high and low-latitude data and model outputs. Simulations of the mid-Pliocene with varying CO_2 concentrations have been proposed for PlioMIP2. These simulations will be performed with the full mid-Pliocene boundary conditions (as described in Table 3.1) and CO_2 concentrations of 350 ppmv (Eoi350), 400 ppmv (Eoi400) and 560 ppmv (Eoi560)(Full description of experiments is given in chapter 3). The simulated outputs will be utilized by investigating if varying CO_2 concentration can account for data-model mismatches. This will be performed by comparing mid-Pliocene sea surface temperatures (simulated at 350, 400 and 560 ppmv, respectively) with mid-Pliocene reconstructions. The influence of varying CO_2 on data-model agreement might have opposing effects for high latitudes (that are modelled too cold in PlioMIP1) and low latitudes (that are modelled too warm in PlioMIP1). It is therefore not expected to find a CO_2 forcing that will lead to an improved agreement between models and reconstructions for both high and low latitudes. This study will test to which extent the uncertainty in CO_2 concentration could contribute to the data-model disagreement in the respective regions. It is not to be ignored that other effects than CO_2 may be an equal or even more important factor

in resolving disagreement between models and the geological records.

1.2 Outline of the thesis

The general structure of this study is as follows. Chapter 2 provides a detailed description of COSMOS, a coupled atmosphere-ocean GCM used in this study. Furthermore, information about the major components of the model, the resolutions are provided and relevant studies that have been carried out using the model are summerized. Chapter 3 describes the full set of boundary conditions for PlioMIP1 and PlioMIP2 (as provided by Haywood et al. (2010, 2011) and Haywood et al. (2016) respectively), and also presents the experimental design as well as methods applied in the analysis of simulation results. Chapter 4 present the simulation results, it consists of five sections which give a detailed analysis of selected PlioMIP2 simulations. The first of the five sections covers the estimation of climate sensitivity for two different geographical configurations namely, the mid-Pliocene and the Pre-industrial (PI). This is followed by analyses of the anomalies in simulated mid-Pliocene atmospheric and oceanic quantities with respect to the PI-control simulation. These anomaly analysis is performed for surface temperature, precipitation, sea surface temperature, sea ice, sea surface salinity and the Atlantic meridional overturning circulation (AMOC). Furthermore, COSMOS simulations for PlioMIP1 are compared with the respective PlioMIP2 simulations by obtaining the anomalies with respect to the PlioMIP1/PlioMIP2 PI-control simulation.

Subsequently, simulated mid-Pliocene SSTs are compared with the reconstruction. In the North Atlantic, PlioMIP1 and PlioMIP2 simulated SSTs are compared to the reconstruction to determine the simulation which is in a better agreement with the geological records. Root mean square error (RMSE) analysis is utilized in determining the mid-Pliocene simulation which agrees better with proxy data. Similarly, RMSE is also utilzed to determine if uncertainty in the concentration of atmospheric CO_2 contributes to data-model discord. Furthermore in Chapter 4, the pattern of the different phases of oscillation in COSMOS simulations under the effect of high CO_2 are identified.

In Chapter 5, discussions about the results described in the previous chapter are presented, while Chapter 6 draws conclusion from all the analysis results and propose an

outlook on possible future challenges.

CHAPTER 2

Model description

The coupled atmosphere-ocean GCM used in producing simulations for this study is known as the Community Earth System Models (COSMOS, version: COSMOS-landveg r2413, 2009), which was developed by the Max Planck Institute for Meteorology (MPI) in Hamburg, Germany. It consists of four major components namely, the ECHAM5 atmosphere model, the MPI-OM ocean model, the land-vegetation and carbon cycle model JSBACH and the ocean biogeochemistry model HAMOCC (the later which will not be used in the simulations utilized in this study). The COSMOS has already been employed to analyse the climate of the Last Millennium (Jungclaus et al., 2010), warm climates of the Miocene (Knorr et al., 2011); the Pliocene (Stepanek and Lohmann, 2012); glacial climates (Gong et al., 2013; Kageyama et al., 2013) and interglacial climates (Varma et al., 2012; Wei and Lohmann, 2012).

2.1 The Atmosphere model ECHAM5

The atmospheric model ECHAM5 (Roeckner et al., 2003) is the fifth-generation atmospheric GCM developed at MPI based on pre-existing spectral weather prediction model

of the European Centre for Medium-Range Weather Forecasts (ECMWF). It earns the first part of its name EC through the development at the ECMWF, and the last part HAM following a comprehensive parameterization package developed at Hamburg. The vertical dimension of ECHAM5 is structured on a hybrid sigma-pressure-level system. ECHAM5 is utilized in T31/L19 resolution, this implies that there are 19 levels present and triangular truncation of the series of spherical harmonics is performed at wavenumber 31. The latter describes the approximation of the solution to a maximum wavenumber. Parameterization are computed on the 96 x 48 real space T31 grid (3.75° x 3.75°) where the dynamics are computed on spectral domain. The atmospheric simulations time step of 2400 s.

In solving the equations for divergence, temperature and surface pressure, ECHAM5 employs a semi-implicit time scheme based on the work of Robert et al. (1972). Furthermore, a semi-implicit method is used in solving the zonal advection terms in the vorticity equation following the results obtained by Robert (1981, 1982). Passive transport tracers are accounted for in the model using a semi-Lagrangian scheme as introduced by Lin and Rood (1996). Horizontal diffusion is formulated in spectral space contrary to the other physical parameterizations which are computed in grid point space. The soil temperature profile is calculated from the thermal diffusion equation. To fully account for the orographic variations on scales smaller than the typical horizontal resolution of climate models, the subgrid scale orographic parameterization scheme of Lott and Miller (1997) and Lott (1999) has been implemented in ECHAM5. The hydrological cycle is represented in ECHAM5 by a high resolution (0.5° x 0.5°) hydrological discharge transport model (HD-model) which has been described by (Hagemann et al., 1998). It simulates the global freshwater transport on the land surface. Lateral water-flow is separated into three flow processes of overland flow, base-flow and river-flow. The HD-model is fed by inputs from surface run-off, drainage from the soil, and inflow from other grid-boxes, respectively.

2.2 The land model JSBACH

The land surface and vegetation model JSBACH (Raddatz et al., 2007) is an extension of the ECHAM5 model which is derived by isolating its land components (Roeckner et al., 2003). The JSBACH runs at a horizontal resolution identical to the atmosphere model ECHAM5.

Table 2.1: Plant functional types (PFTs) considered in JSBACH simulations. The rightmost column indicates the class of vegetation (forest or grass) a PFT contributes to as defined by Stepanek and Lohmann (2012).

PFT index	Description	types: forest (F) or grass (G)
1	tropical broadleaved evergreen forest	F
2	tropical deciduous broadleaved forest	F
3	temperate/boreal evergreen forest	F
4	temperate/boreal deciduous forest	F
5	rain green shrubs	G
6	cold shrubs (tundra)	G
7	C3 perennial grass	G
8	C4 perennial grass	G

Plant functional types (PFTs) are used in land models to denote different species of plants which are similar in structure, physiology and phenology. These PFTs can be prescribed by their respective land cover fraction parameters and the maximum vegetated cell area fraction. JSBACH has been developed with thirteen PFTs which describes different deciduous and evergreen trees, crops, shrubs, grasses and pastures of which eight (Table 2.1) are used for the model runs discussed in this study. The JSBACH has the capability of simulating dynamic changes in the distribution of vegetation caused by changes in ambient climatic conditions (Brovkin et al., 2009). While the vegetation was prescribed for mid-Pliocene conditions in PlioMIP1, it is free to change and impact on climate variations in PlioMIP2.

2.3 The ocean model MPI-OM

The ocean model MPI-OM (Marsland et al., 2003) is an ocean general circulation model (OGCM), and a successor of the Hamburg Ocean Primitive Equation model (HOPE). The model dynamics are solved on an orthogonal, curvilinear C-grid (Arakawa and Lamb, 1977), which is an improvement on the previously used staggered E-grid (Marsland et al., 2003). The MPI-OM is based on a curvilinear, bipolar grid with north and south poles over Greenland and Antarctica, respectively. It has a formal resolution of 3.0° x 1.8° (GR30) and spread over 40 unequally spaced z-coordinate model levels.

The MPI-OM contains a dynamic-thermodynamic sea ice model of Hibler (1979) which

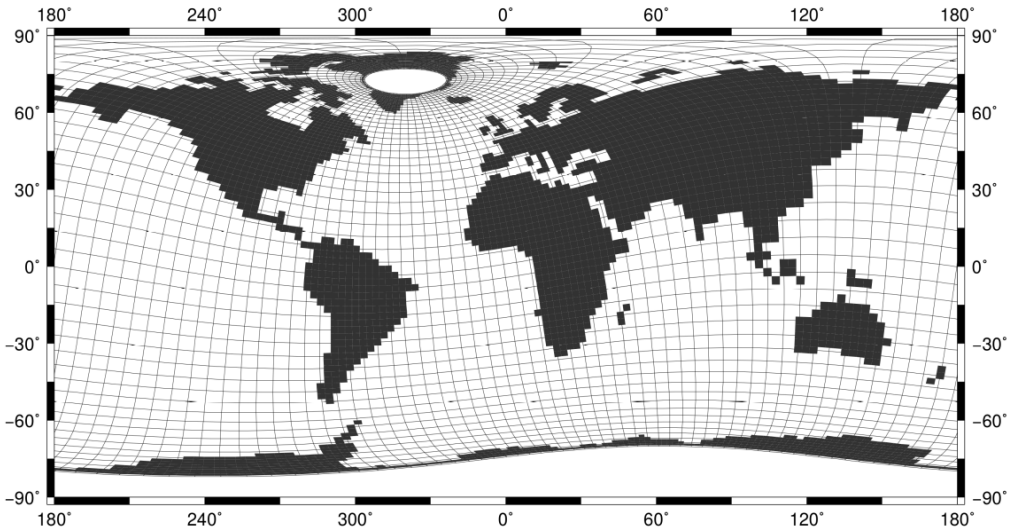

Figure 2.1: Land-sea distribution on the ocean model grid, showing two poles over Greenland and Antarctica (Figure adapted from Stepanek and Lohmann, 2012).

simulates sea ice thickness and its distribution in dependence of ambient climatic conditions. Flow across steep topography is parameterized following the boundary layer scheme as described by Beckmann and Döscher (1997), Lohmann (1998) and Legutke and Maier-Reimer (2002). Eddy-induced mixing is parameterized following Gent et al. (1995). Furthermore, overturning by convection is parameterized via increased vertical diffusion (Jungclaus et al., 2006). An isopycnal scheme is applied for subgrid scale mixing (Marsland et al., 2003). The time step for the model run is 8640 s with no flux adjustments.

CHAPTER 3

Data and methods

3.1 Boundary conditions

Creating boundary conditions for past time periods is one of the most time consuming tasks faced in paleoclimate modelling. These boundary conditions consider at least, the continental configuration derived from plate tectonic modelling as well as topography and bathymetry (Sewall et al., 2007). Furthermore, derivation of vegetation distribution may be necessary if such is not modelled itself. Assumptions with respect to paleoclimate boundary conditions can vary from researcher to researcher, and the Pliocene is not an exceptional time slice in this respect. Therefore, to provide common grounds for the model intercomparison, the PlioMIP provide sets of boundary conditions that will be implemented consistently across ensemble models in simulating the mid-Pliocene Warm Period (mPWP). This is to enhance the knowledge of the mPWP climate as well as study its potential relevance in the context of future climate change.

3.1.1 PlioMIP1

The boundary conditions used in PlioMIP1 to simulate the mid-Pliocene climate were derived from the PRISM3D dataset (Dowsett et al., 2010), which is an improvement of the PRISM2 reconstruction of Dowsett et al. (1999). Contrary to the land-sea mask presented in PRISM2, the PRISM3D land-sea mask is fractional. Continental and oceanic regions are 100% land and ocean respectively, but the margin between these areas is fractional. Grid cells covered by land are characterized as land cover and topography (Haywood et al., 2010, 2011). For regions covered only by ocean, ocean temperatures are reconstructed.
The PlioMIP1 dataset contains reconstructions of SST, deep ocean temperature (DOT), vegetation, ice sheets and topography. The PRISM3D DOT reconstruction is presented at a 4° x 5° resolution with 33 depth layers. The mPWP vegetation pattern is reconstructed from 202 paleobotanical sites as described by (Salzmann et al., 2008). Vegetation land cover types are provided on fractional land grid so that every cell with any fraction of land has a land cover type. The topography reconstruction of Sohl et al. (2009) is based on a 25 m higher sea level, thus the topography were derived from this reconstruction (Haywood et al., 2011). For the mid-Pliocene simulation of PlioMIP1, concentration of atmospheric CO_2 was prescribed to be 405 ppmv across all model ensembles. All other trace gases and aerosols, which includes nitrous oxide (N_2O), methane (CH_4), chlorofluorocarbons (CFCs) and O_3 were set to the corresponding values specified for the pre-industrial simulation by individual participating groups.
As documented for COSMOS by Stepanek and Lohmann (2012), atmospheric CO_2 for the PI-control simulation was set to 280 ppmv, CFCs were assumed to be absent while N_2O and CH_4 were set to 270 ppbv and 760 ppbv respectively. Earth's orbital parameters were prescribed as constant values of eccentricity (0.016724), obliquity (23.446°), and length of the perihelion (282.04°). The Solar constant was used as prescribed in the standard setup of COSMOS for standalone atmosphere (1365W/m^2) and coupled atmosphere-ocean simulations (1367 W/m^2). The land-sea mask of the PI-control simulation was also implemented for the mid-Pliocene simulation with the exception of the Hudson Bay, which was open in the PI-control but closed for the mid-Pliocene. Furthermore, adjustments at the Western Antarctic continent were implemented for the mid-Pliocene simulation.

3.1.2 PlioMIP2

The datasets provided for setting up PlioMIP2 simulations contain palaeogeography data which includes land-sea mask, topography, bathymetry, land ice, and the state of ocean gateways. Furthermore, it also contains vegetation, lakes, soils and river which were all provided by the PRISM4 project of the US geological survey (Haywood et al., 2016). The main aim of PRISM4 as described by Haywood et al. (2016), is to increase the temporal resolution of proxy records, and to concentrate on a smaller interval of time approaching a time slice reconstruction for Marine Isotope Stage (MIS) KM5c. This makes it possible to provide more certain values for astronomical and orbital forcing as a pre-condition for improved model-data comparison. The KM5c time slice (Figure 3.1) was selected partly on the basis of a strong similarity in orbital forcing to present day (Haywood et al., 2016). The palaeogeography datasets are given at a 1° x 1° resolution in NetCDF format. The NetCDF datasets provided to facilitate simulations in PlioMIP2 are classified in two different categories namely the Pliocene enhanced and Modern standard datasets. The former is utilized for simulation in this study.

Pliocene enhanced datasets result from the PRISM4 Pliocene palaeogeography reconstruction. These include topography, bathymetry, ice sheets and landsea mask. On the other hand, the Modern standard datasets are derived from ETOPO1. They consist of a modern geography, including present-day topography, bathymetry, ice sheets and landsea mask. This data is used to create the Pliocene setup via anomaly method as outlined in Haywood et al. (2016). The PRISM4 palaeogeography takes into consideration the influence of processes that affect sea level and surface topography. These processes include variations in the mantle flow which are associated with changes in dynamic topography (Rowley et al., 2013), and global isostatic adjustment based on Raymo et al. (2011), which is due to ice un-loading and used to predict global land sea distribution based on reconstructed topography. These two processes were previously not taken into account in the PRISM3D reconstruction of Sohl et al. (2009).

Ocean gateways remain the same as utilized in PlioMIP1, except for the Bering Strait and the Canadian Arctic Archipelago, which both are to be closed in PlioMIP2 (compare Figure 3.2a and b). Similarly, the Canadian Arctic Archipelago will be closed isolating

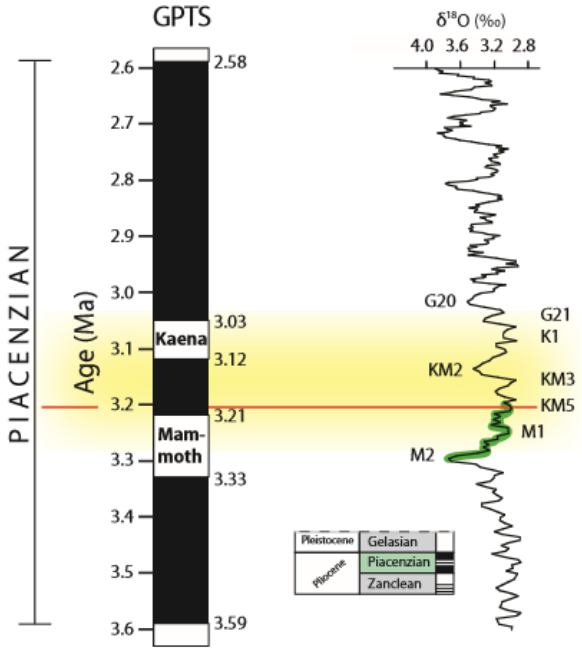

Figure 3.1: Benthic δ^{18}O record from Lisiecki and Raymo (2005) showing the position of the PRISM3 time slice (yellow shading) and extent of the PRISM4 interval (green coloured section of LR04) between Marine Isotope Stages (MIS) M2 and KM5. PlioMIP2 time slice (3.205 Ma) is shown by the red line (Haywood et al., 2016)

Baffin Bay and the Labrador Sea from the Arctic Ocean. Due to unavailability of a near-perfect global vegetation dataset for the Pliocene, a fixed reconstruction of vegetation has to be prescribed for mid-Pliocene simulations. The vegetation classes of the land and vegetation model JSBACH are not similar to the PRISM4 Pliocene reconstruction dataset. In order to fully account for vegetation in the simulations, the dynamic vegetation module of JSBACH is turned on.

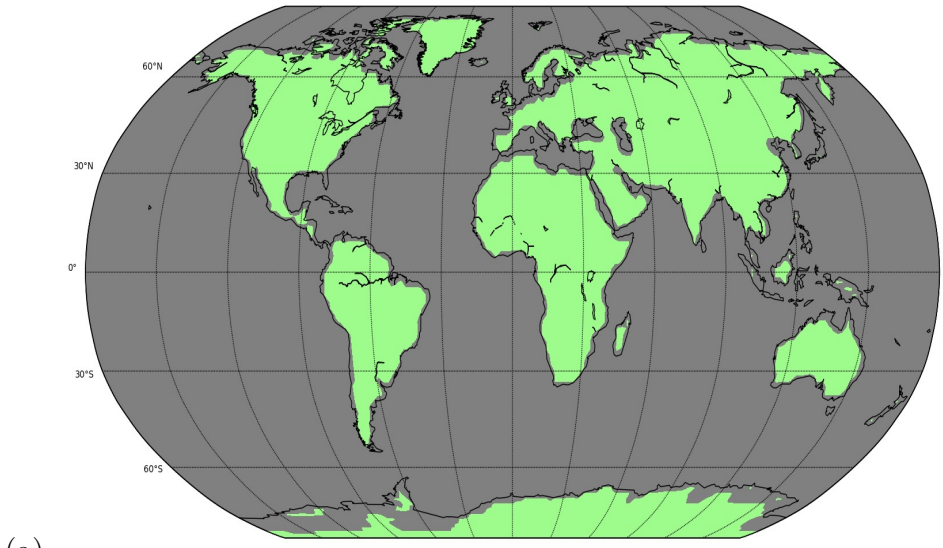

(a)

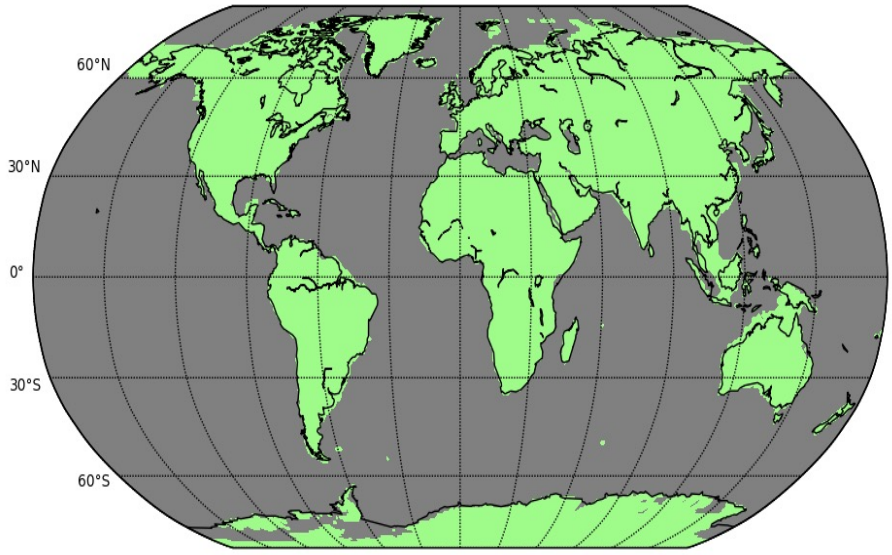

(b)

Figure 3.2: (a) Land sea mask utilized in PlioMIP1 simulations as prescribed by Haywood et al. (2010), assuming an open Bering Strait. (b) show the Land-sea mask prescribed for PlioMIP2 simulations with closed Bering Strait as described in Haywood et al. (2016). The land area are represented as green while the grey denotes the oceans.

3.2 Experimental design

Experiments are carried out and named according to PlioMIP2 specifications presented by Haywood et al. (2016). Simulations are based on various boundary conditions associated with prescribed topography, ice-sheets, soil, lakes and CO_2 concentration. For easier comparison, simulations are denoted by abbreviations following the naming convention described in the PlioMIP2 protocol. All simulations take an abbreviated form, "Exc", where c is the concentration of atmospheric CO_2 in ppmv and x refers to any boundary conditions which are indicative of Pliocene conditions such that x can be o for changes in topography, lakes, soils, or i for changes in ice sheets. In a more detailed form, a simulation in which all the boundary conditions are set to Pliocene conditions and with a prescribed atmospheric CO_2 concentration of 400 ppmv will be denoted as Eoi400. A simulation, with partly Pliocene and partly PI conditions will take another form. For example, a simulation with Pliocene ice sheets, PI topography and prescribed atmospheric CO_2 concentration of 560 ppm, will be denoted as Ei560. The details of all simulations proposed for PlioMIP2 are given in Table 3.1 with dynamic vegetation specified across all simulations.

Eoi400 is the CORE PlioMIP2 mid-Pliocene simulation, while E280 is the CORE Pre-Industrial reference state. Other simulations study the impact of modifications of forcing and boundary conditions in the model.

The orbital forcings utilized in the simulations are the Pre-Industrial values specified for PMIP4 adapted from Otto-Bliesner et al. (2016). Earth's orbital parameters are prescribed as constant values of eccentricity (0.0167643), obliquity (23.459277°) and the length of perihelion (280.32687°). Concentration of traces gases such as CH_4 and N_2O, are set to 808 and 273 ppmv, respectively.

It is important to note that simulations Eo280, Ei280, Eo400, Ei400 and Eoi450 are not utilized in this study due to limited time frame of conducting and writing a master thesis.

Table 3.1: PlioMIP2 proposed simulations with Modern (Mod) and Pliocene (Plio) boundary conditions (Haywood et al., 2016). Dynamic vegetation is specified across all simulations.

ID	Description	LSM	Ice	Lakes	Topography	Soil
Eo280	PI simulation with topography set to Pliocene values outside ice-sheet regions	Mod	Mod	Plio	Plio	Plio
Ei280	PI simulation with ice configuration set to Pliocene on Greenland and Antarctica.	Mod	Plio	Mod	Mod	Plio
Eo400	Pliocene simulation with ice-sheet on Greenland and Antarctica set to modern.	Mod	Mod	Plio	Plio	Plio
Ei400	Pliocene simulation with topography outside the ice-sheet lakes set to modern.	Mod	Plio	Mod	Mod	Mod
Eoi280	Pliocene simulation	Mod	Plio	Plio	Plio	Plio
Eoi350	Pliocene simulation	Plio - Mod	Plio	Plio	Plio	Plio
Eoi400	Pliocene simulation	Plio - Mod	Plio	Plio	Plio	Plio
Eoi450	Pliocene simulation	Plio - Mod	Plio	Plio	Plio	Plio
Eoi560	Pliocene simulation	Plio - Mod	Plio	Plio	Plio	Plio

3.3 Methods

3.3.1 Estimation of Climate Sensitivity

To determine whether CS is dependent on the background climate and state of the underlying boundary conditions, two different background geographies are studied. PI simulation with prescribed CO_2 level of 280 ppmv, and perturbed simulation with 560 ppmv were carried out respectively. Furthermore, the mid-Pliocene climate is also employed for deriving CS. Simulations with mPWP boundary conditions are carried out with different CO_2 levels of 280, 400 and 560 ppmv respectively. By carrying out these experiments, it has been ensured that CO_2 is constant across the two climate states leaving the difference between the two climate states as the geographical boundary conditions. The CS is estimated following the method of Chylek and Lohmann (2008), and it is expressed mathematically as

$$CS = \frac{\Delta T}{\Delta F} \tag{3.1}$$

where ΔT is the difference between average global Surface Air Temperatures (SAT) of two equilibrium climate states, and ΔF is the sum of all forcings that cause the difference between the two climate states. In the framework of PlioMIP2, the specified concentration of CO_2 accounts for the total greenhouse gases forcing derived from all sources (Haywood et al., 2016). Thus, Arrhenius's greenhouse law for CO_2 is adopted for the greenhouse forcing stated by Walker (2010) as,

$$\Delta F = \lambda * ln\frac{C}{C_0} \tag{3.2}$$

where C_0 denotes the concentration of CO_2 specified for the PI-control simulation, which in this study is 280 ppmv, and C refers to the changed CO_2 concentration in the atmosphere with respect to C_0, which amounts to 560 ppmv. Using the approximation of Myhre et al. (1998), λ is a constant factor of 5.35 W/m^2. Typically, CS is given in the unit of K/Wm^{-2} which specifies the equilibrium temperature change (K) per unit change of the radiative forcing (W/m^2). CS is usually defined for the doubling of CO_2 by combining equations 3.1 and 3.2 such that

$$CS = \frac{\Delta T}{\lambda * ln\frac{C}{C_0}} \tag{3.3}$$

which gives an estimate of long-term temperature response to doubled CO_2 concentration. It is however important to note that the estimate of CS in this context is a characteristic for simulations with a specific model and does not refer to the particular set up or initialization procedures prescribed for PlioMIP2.

3.3.2 Statistical analysis

The statistical significance of anomalies of atmospheric and oceanic quanties are tested. Significance tests are performed for 100-year climatologies of all the quantities considered. This analyses are carried out for two seasons namely, boreal winter and boreal summer. The significance in the annual changes is also tested. Seasonal analysis is not performed

for oceanic quantities due to a near vanishing seasonal cycle exhibited by these quantities. Statistical significance of anomalies accounts for the effective degrees of freedom based on autocorrelation following the method of Dawdy and Matalas (1964).

According to Dawdy and Matalas (1964), effective degree of freedom utilized in the analyses ensure that each event considered in the selected time series are independent of the preceding and the following events.

Agreement between COSMOS simulated SST and reconstruction is assessed using the Root Mean Square Error (RMSE). The error at a specific location is calculated as the difference between SST as estimated from COSMOS and as derived from the reconstruction at the same location. The global RMSE for the model results is then calculated as

$$RMSE = \sqrt{\frac{1}{N}\sum_{i=1}^{N}(x_i^m - x_i^r)^2} \tag{3.4}$$

where $x^m{}_i$ and $x^r{}_i$ represents COSMOS simulated (m) and reconstructed (r) SST at location i, respectively. N is the number of locations where SST reconstructions are available.

CHAPTER 4

Results

In the analysis of the simulation results from pre-industrial and mid-Pliocene geography, annual mean SSTs, obtained from all simulations on the global scale are compared. Figure 4.1a shows the time evolution of SST in the perturbed CO_2 experiments with the E280 (red), hereafter referred to as PI-control simulation, and E400 (blue), hereafter referred to as PI-modern. The latter is named PI-modern because the CO_2 concentration is somewhat similar to that of the modern day coupled with PI geography. E560 and E600 denote the simulations with 560 and 600 ppmv and with PI geography, respectively. E280, E400 and E560 were carried out for modern geography with respect to PlioMIP's prescription while the E600 simulation is performed to get a better impression of the effect of small changes in CO_2 for extreme CO_2-simulations and it is not prescribed by PlioMIP. On the other hand, the blue line in Figure 4.1b shows the time evolution of SST in the mid-Pliocene simulation (Eoi400) with the best guess of Pliocene CO_2 as published by Haywood et al. (2016). Eoi350 and Eoi560 in yellow and green (see Figure 4.1b) are used in this study to ascertain the extent to which the uncertainty in the level of atmospheric CO_2 can contribute to the lingering issues between data and model outputs.

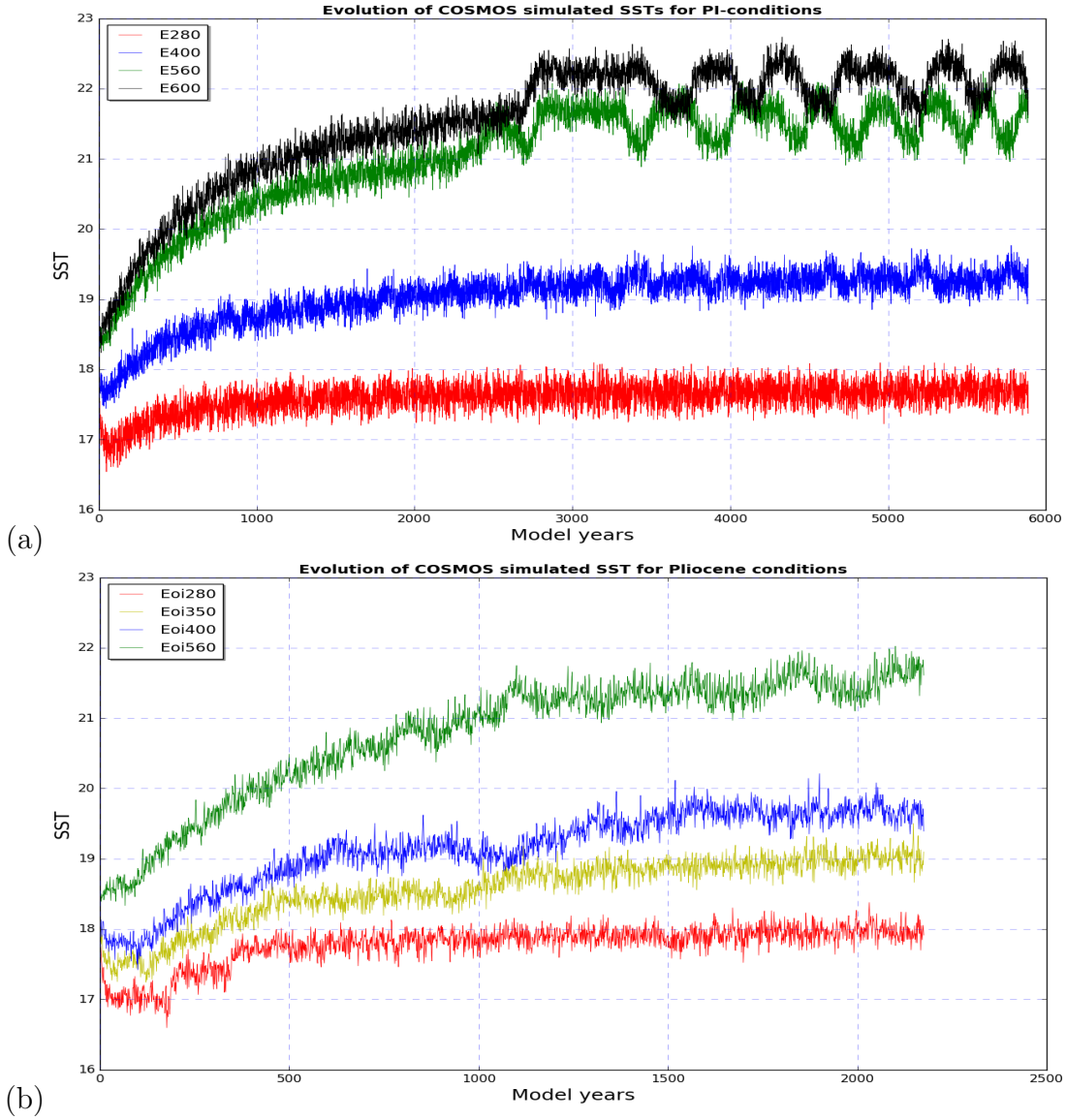

Figure 4.1: Time evolution of globally averaged annual sea surface temperature (SST) in °C, for Pre-industrial (PI) geography (a) and Pliocene geography (b). Line colors specify differences in the CO_2 concentration for each simulation, with red denoting the simulations with 280 ppmv. Yellow, blue, green and black represent simulations with 350, 400, 560 and 600 ppmv, respectively

E280 and E400 simulations show a stable trend after 2,000 modelled years. The trend continues on a long-term for E280, while the E400 experienced a sinusoidal shaped oscillation after about 3,200 modelled years. The amplitude of the oscillation is more pronounced for simulation E560 and E600. Potential regions of origin as a precursor to identify potential cause of these oscillations between cold and warm global average conditions will be identified in section 4.5 of this chapter.

Simulation Eoi400 as shown in Figure 4.1b, shows a more stable trend than other simulations except for E280, which also show a stable trend from model year 3,200 onwards. It is evident that the COSMOS simulate warmer mid-Pliocene SSTs in comparison to the PI-control, with PI-control recording an annual average of 17.59°C while the mid-Pliocene simulation gives an annual mean of 19.41°C which implies a warming of 1.82°C. Changes in climatic variables from PI-control simulation to the mid-Pliocene simulation form the basis of most of the analysis carried out in this chapter. Only the time period, in which all simulations are well equilibrated is considered, namely model years 2000-2099. This time period is not overlapping with the oscillations noticed in simulations with high CO_2. Therefore, it is considered to be suitable for making inferences about changes in climatic variables of the COSMOS simulated mid-Pliocene climate.

4.1 Quantification of CS

Determination of the dependency of CS on the state of the earth surface and the bathymetry is performed by means of PlioMIP2 mid-Pliocene-geography-based (Eoi-simulation) and Pre-Industrial-geography-based (E-simulations) with 280 and 560 ppmv of CO_2.

E280 and E560 were used to account for the change in temperature and CS for PI-ensemble, while Eoi280 and Eoi560 were used to determine corresponding values for the mid-Pliocene ensemble.

Table 4.1: Climate sensitivity estimates for different background climates

Climate state	CS (K)	CSW (K/Wm^{-2})
mid-Pliocene	4.5	1.21
PI	4.2	1.13

Table 4.1 shows the result obtained for both ensembles with mid-Pliocene set-up having a CSW of 1.21, while a CSW of 1.13 is obtained for the PI model set-up, resulting in a difference of 0.08 K/Wm^{-2} between the different ensembles.
Furthermore, changes in temperature in response to a doubling of CO_2 which is commonly referred to as the CS in the climate modelling community, is estimated for both ensembles. A climate sensitivity of 4.5 K per doubling of CO_2 is found for the mid-Pliocene model set-up, while the corresponding CS value in the PI ensemble is 4.2 K per doubling of CO_2.
The obtained results confirm that CS is indeed dependent on the geography as prescribed by Haywood et al. (2016). These results further confirm that warm climates are more sensitive to a change in CO_2 level than cold climates in agreement with the findings of Friedrich et al. (2016).

4.2 Spatial and seasonal variation of PlioMIP2 mid-Pliocene anomalies of atmospheric and oceanic quantities

4.2.1 Surface air temperature

The best guess mid-Pliocene (Eoi400, Haywood et al. (2016)) simulation differs significantly from the PI-control simulation in terms of the configuration of sea-ice, orography and land-sea mask. Seasonal and spatial consideration of surface air temperature (SAT) provides a suitable means of identifying seasonal and regional dependency and the impacts of the implemented mid-Pliocene forcing where SAT is strongly influenced by the implementation of the PlioMIP2 mid-Pliocene forcing and boundary conditions.

Generally, stronger temperature differences occur over continents than over oceans due to the lands tendency to heat-up more rapidly than the ocean due to its lower heat capacity. Eurasia experiences a more pronounced warming than other continents, in particular during boreal winter from around 45°N extending to the Arctic region but with an exception of Japan, where a gradual cooling is noticed during the boreal winter and on the annual mean (compare Figures 4.2a, b, and c).

For the Hudson Bay, a strong temperature variation, showing different pattern and intensity on the annual and seasonal basis is observed. There is a boreal summer warming in this region (Figure 4.2b), while during boreal winter, cooling is predominant (Figure 4.2c). On the other hand, annual mean temperature remain largely unchanged (Figure 4.2a). The observed seasonal variation over the Hudson Bay is due to the prescribed change in the land-sea mask between the PlioMIP2 mid-Pliocene and the PI-control model setups. The mid-Pliocene simulation is characterized by a land-sea mask in which the Hudson Bay is replaced by land while it is part of the sea in the setup of PI-control

simulation. Positive and negative SAT anomalies recorded over Hudson Bay are therefore due to land-sea contrast in heat capacity. This land-sea contrast occurs partly as a result of the different thermal inertias of the land and ocean, with mixing of heat downwards taking place in the ocean, while heat is stored on land preliminary or the surface. Naturally without considering the simulation results, summer is drier than winter, so less clouds are formed during summer. Therefore, the scattering, reflection and absorption effect of clouds is rather small during summer, allowing more shortwave radiation to reach the surface. Enhanced warming due to this effect explains the positive anomaly recorded over the Hudson Bay during summer months, and vice-versa during winter.

Furthermore, increased warming is noticed in the polar regions, a phenomenon usually referred to as polar amplification. This observed polar warming is more intense during boreal winter (Figure 4.2c) in the Arctic region than during the respective boreal summer (Figure 4.2b). Over Greenland, significant warming is present due to significant changes in surface albedo caused by the reduction of land-ice in the mid-Pliocene simulation and reduction in surface elevation. A SAT anomaly of 26.03 K is found during the boreal summer over Greenland, which is the highest temperature anomaly present among the considered COSMOS simulations. A minimum temperature anomaly of -10.9 K is observed during boreal winter.

However, it is of relevance to identify the main factor driving SAT variations in the mid-Pliocene setup of PlioMIP2. This is done by isolating anomalies that occur through the variation in atmospheric CO_2, i.e. via comparing simulations Eoi400 and E400, that have the same atmospheric CO_2 concentration. Contrary to the Eoi400 simulation, which is based on PlioMIP2 mid-Pliocene configuration with prescribed orography and land-ice, E400 is mainly of the pre-Industrial geography and atmospheric CO_2 concentration of 400 ppmv. From the anomaly analysis between simulations Eoi400 and E400 (Figure 4.3), the polar warming observed by comparing the Eoi400 with the E280 simulations (Figure 4.2) can solely be attributed to the CO_2 difference between the two simulations. Similarly, the gradual warming noticed in the latter over the ocean, is greatly reduced (Figure 4.3). Anomalies between simulations Eoi400 and E400, show the maximum SAT

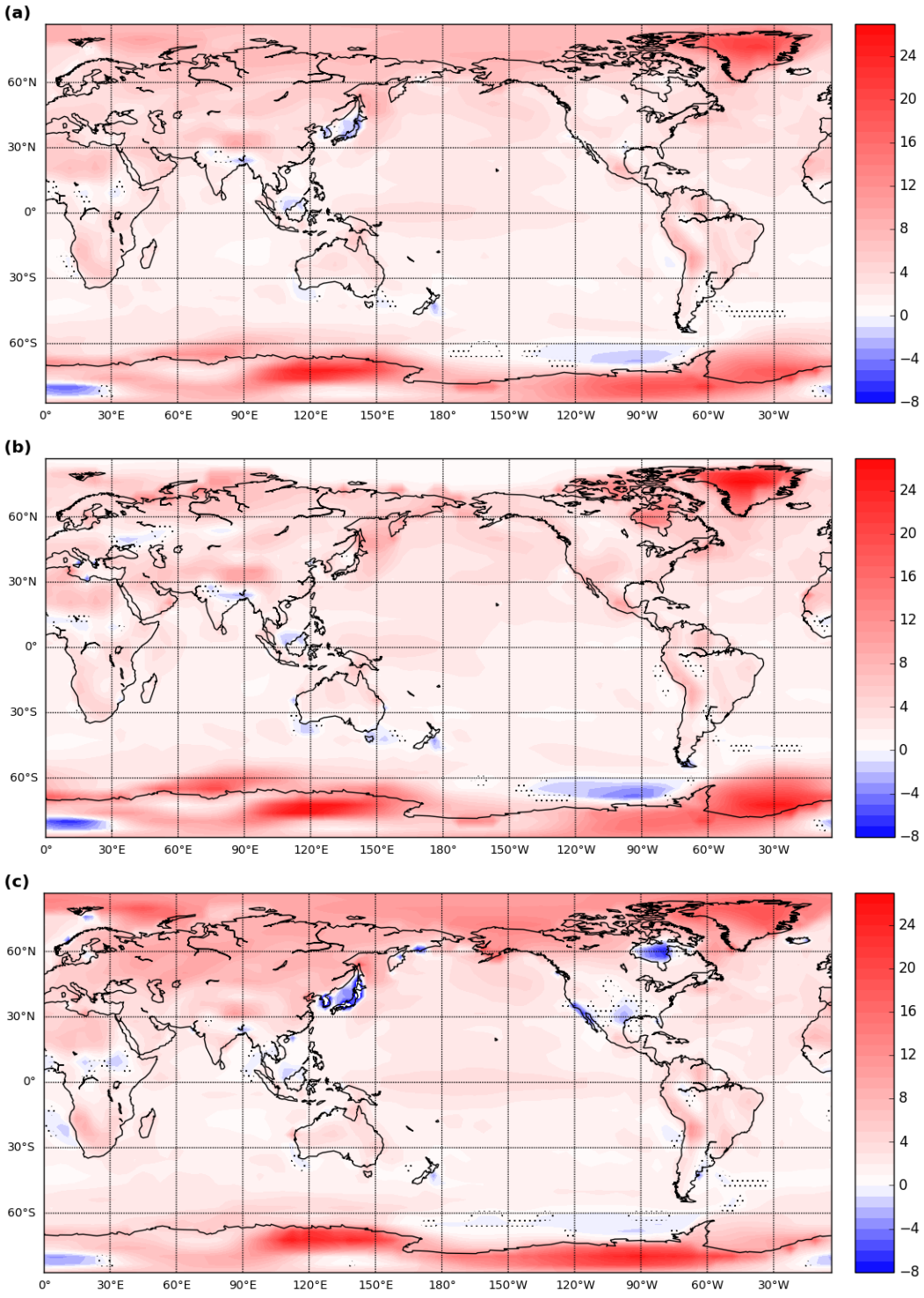

Figure 4.2: Surface air temperature anomalies in °C between mid-Pliocene (Eoi400) and PI-control (E280) simulations. Shown are annual mean (a), boreal summer season (JJA) (b), and boreal winter season (DJF) (c), retrieved from 100-year time series of model output. Strong temperature anomalies over the Hudson Bay are caused by change in the land-sea mask. Stipples (black dots) show regions of statistically insignificant differences.

anomaly of 21.25 K during boreal summer, this gives a difference of 4 K between the maximum found by comparing simulations Eoi400 with E280.

Figure 4.4 shows the annual and seasonal variation of the zonal mean SAT across all latitudes. The effect of CO_2 is seen to be fairly constant around the equatorial region with CO_2 causing a warming of 2 K (Figure 4.4c), and a gradual increase noticed in the higher latitudes of the Northern Hemisphere from about 50°N reaching a maximum of about 8 K during boreal winter. On the annual basis, the warming is around 7 K, while the case is different for boreal summer when a rapid cooling is recorded towards the pole. The sequence is different for the Southern Hemisphere, where the change is strongest during boreal summer and weakest during boreal winter with 7 K and 3.91 K respectively. The annual change due to increased CO_2 in this region is 4.9 K.

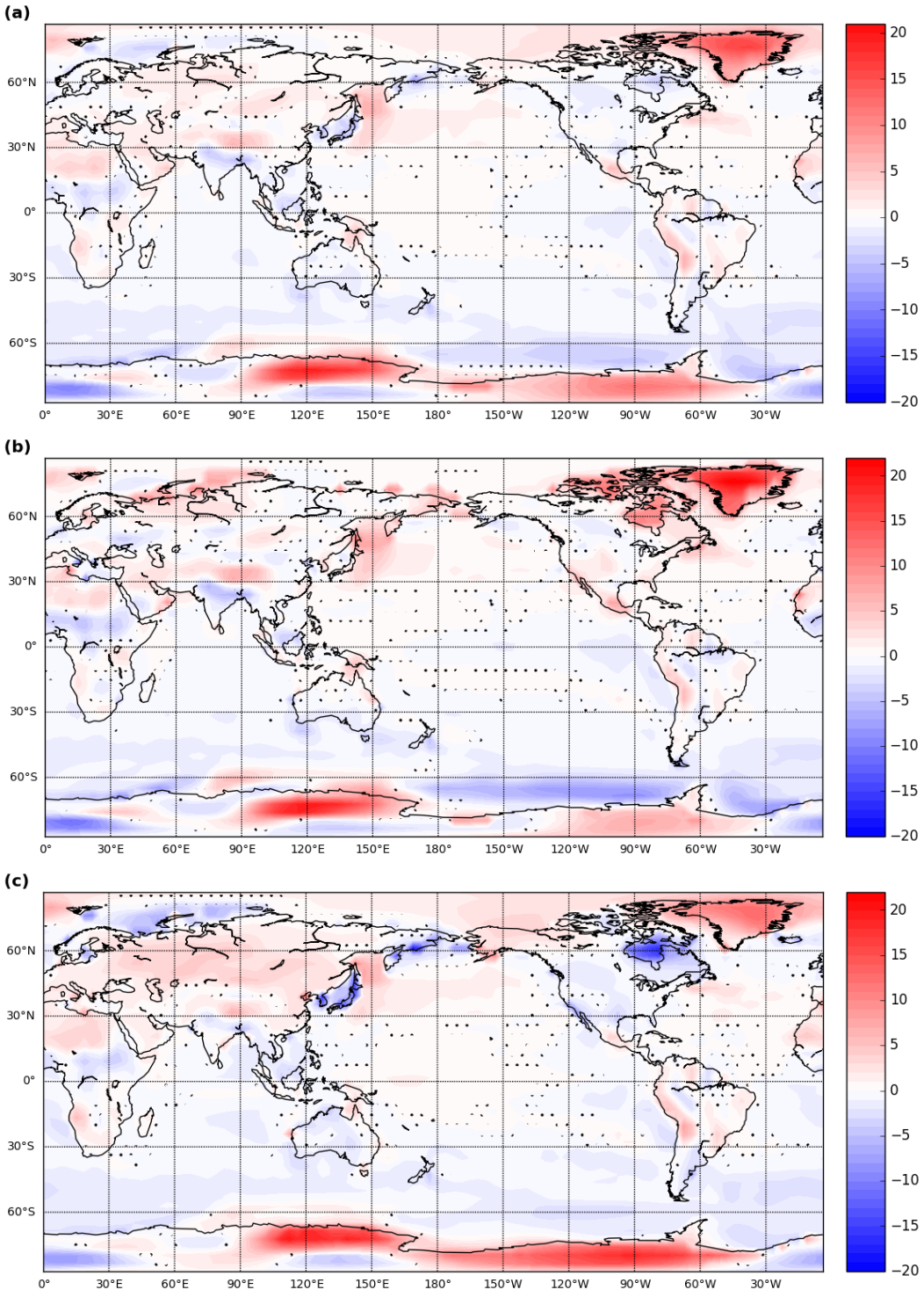

Figure 4.3: Surface air temperature anomalies in °C between mid-Pliocene (Eoi400) and PI-modern(E400) simulations. Shown are annual mean (a), boreal summer (JJA) (b), and boreal winter (DJF) (c), retrieved from 100-year climatologies. Stipples (black dots) show area of statistically insignificant changes.

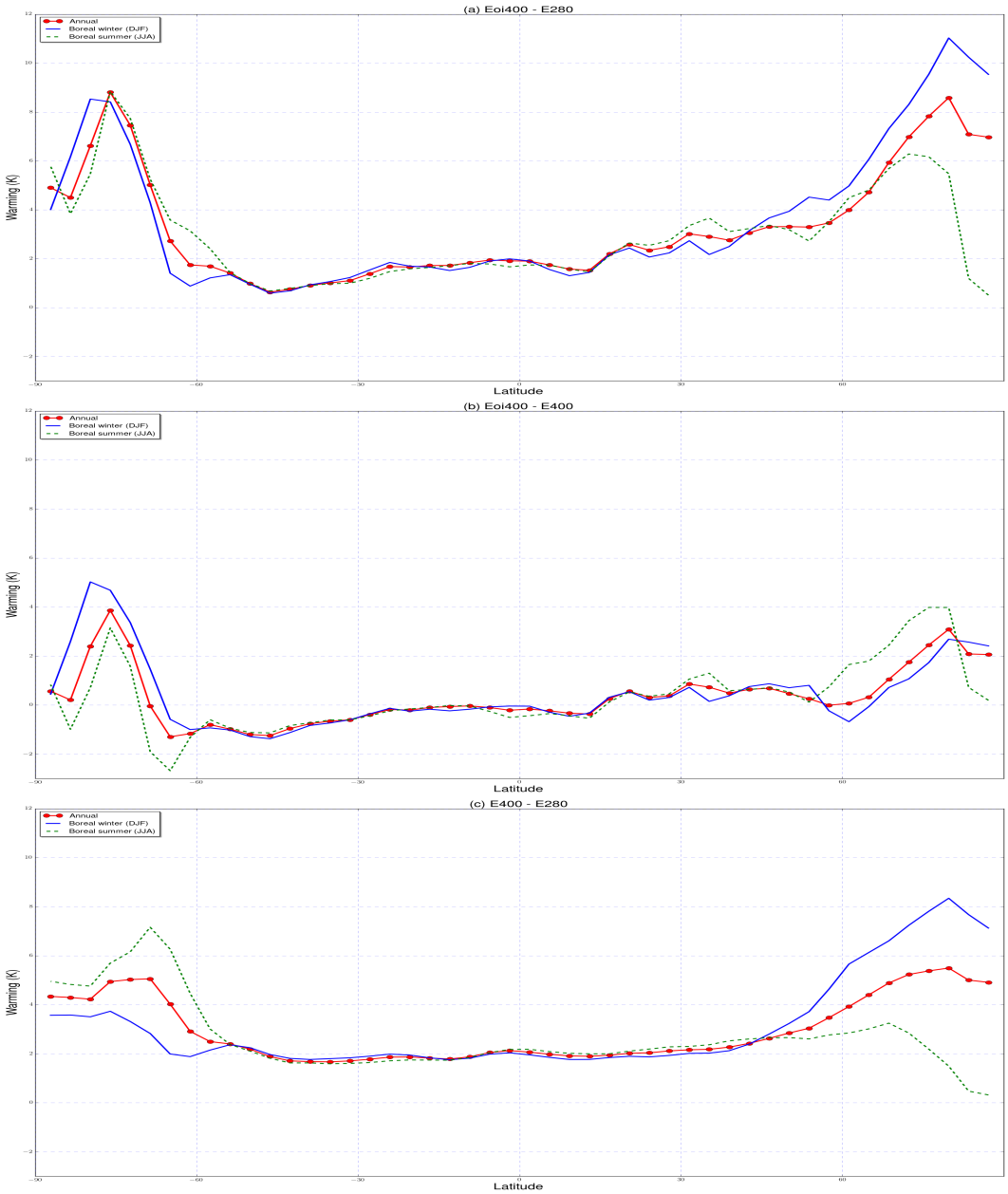

Figure 4.4: Annual and seasonal zonal mean surface temperature changes over 100 model year between mid-Pliocene (Eoi400) and PI-control (E280) simulations (a), and zonally averaged annual mean, winter and summer surface temperature differences between the mid-Pliocene (Eoi400) and PI-modern (E400) (b). (c) is difference between (a) and (b) to account for the zonal warming due to increased CO_2 level. The dashed green line and the blue line show the changes during boreal summer and boreal winter, respectively while the red dotted line describe the annual mean latitudinal variations.

4.2.2 Sea Ice

For the analysis of sea ice, the definition of seasons is different from the conventional December to February (boreal winter) and June to August (boreal summer). Boreal winter is defined as February to April (FMA), and boreal summer as the months of August to October (ASO). According to Howell et al. (2016), these are the three months in which more than half of the PlioMIP1 ensemble simulations show the highest and lowest mean sea ice extents respectively.

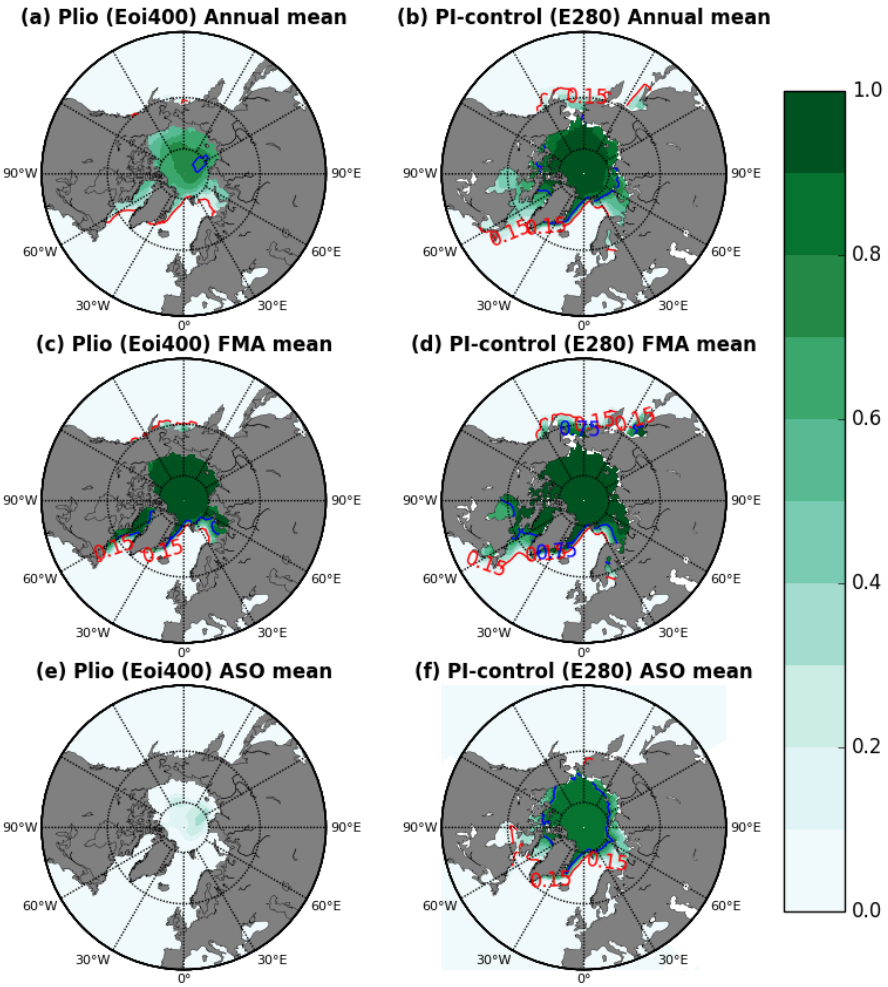

Figure 4.5: Annual and seasonal mean sea ice compactness averaged over 100 model years as simulated by COSMOS for mid-Pliocene (Eoi400) and PI-control (E280). (a), (c) and (e) show annual, winter (FMA) and summer (ASO) averages for Eoi400, while (b), (d) and (f) show annual, winter (FMA) and summer (ASO) averages for E280, respectively. The red contours indicate 15% isoline of sea ice cover while blue contours indicate 75% isoline of sea ice cover. Missing data at the pole is a plotting artifact.

With prescribed PlioMIP2 Pliocene geography and CO_2, COSMOS simulates a considerably smaller sea ice extent in the mid-Pliocene (Eoi400) with respect to the PI-control simulation. The most obvious loss of sea ice is seen around the Hudson Bay (Figure 4.5 (a), (c) and (e)) which is closed and represented as land in the mid-Pliocene simulation . The Canadian Arctic Archipelago is also totally free of sea ice during the mid-Pliocene, as it is also closed in our Eoi400 simulation. In addition to these trivial changes in sea ice, little or no sea ice is present around the Bering Strait during mid-Pliocene boreal winter, but a more pronounced sea ice extent is present in the PI-control simulation (E280). The mid-Pliocene Arctic ocean is sea ice free during the previously defined boreal sea ice summer season, with sea ice compactness dropping below 15% in most regions (Figure 4.5c). This is a combined effect of the imposed mid-Pliocene geography and the increased CO_2 concentration in simulation Eoi400. During winter, the compactness and spatial extent of sea ice are at the highest for both Eoi400 and E280. In the annual mean, the simulated sea ice is gradually reduced from the pole towards the coastlines for simulation Eoi400.

4.2.3 Precipitation

Anomalies of precipitation are shown for annual mean (Figure 4.6a), boreal summer (JJA, Figure 4.6b) and boreal winter (DJF, Figure 4.6c). Generally, the variations of precipitation between the mid-Pliocene (Eoi400) and PI-control (E280) differs greatly between ocean and continents, with the ocean experiencing a more pronounced variation all year round.

Over the Pacific Ocean, there are spatial variation of increased and decreased precipitation rate across all latitudes. These variations extend towards the continents of North and South America, Eurasia and Australia. The anomaly over North America forms a dipole of increased precipitation in the northern part and reduced precipitation in the southern part of the Pacific coast of North America. The variation decreases from the coastline during boreal winter and boreal summer.

A pronounced annual mean variation is shown over South America, with a dipole of increased and decreased precipitation rates in the northern part of the continent, and the southern part during boreal winter, respectively. During boreal summer, a reduced

precipitation rate is witnessed over South America. Annual and boreal winter mean over the Greenland show increased wetness along the eastern coast with a shift to the center during boreal summer. Over the Eurasia, drying of the Tibetan Plateau occurs all year round. Meanwhile, precipitation rates over Eurasia are largely unchanged with few exceptions. Increased precipitation for mid-Pliocene with respect to the PI-control is present in the north western part and the eastern part in the annual mean, and also over India during boreal summer. There is increased and decreased rainfall north and south of the equatorial Pacific while in regions close to the landmass of the Caribbean Islands, decreased precipitation prevails. The Indian Ocean is also characterized by increased and decreased precipitation patterns mainly around the equator. Annual mean precipitation pattern shows increased dryness towards the Western Caribbean and increased wetness towards the coast of East Africa. Seasonal pattern over the Indian ocean differs completely from the annual pattern with the former showing a signal of the Inter-Tropical Convergence Zone (ITCZ). The southern part of Africa receives more precipitation in our mid-Pliocene (Eoi400) simulation in comparison to the PI-control (E280) on the annual basis, but with the exception of South Eastern Africa.

In the northern Hemisphere zonal mean (Figure 4.7), COSMOS simulates a higher precipitation rate all year round for mid-Pliocene in comparison to the PI-control simulation, with an exception for regions between 25°N - 40°N where the zonal averages for PI-control exceed that of the mid-Pliocene. Similarly, in the mid-Pliocene higher precipitation is also present in the Southern Hemisphere, with obvious exception of the tropical latitudes.

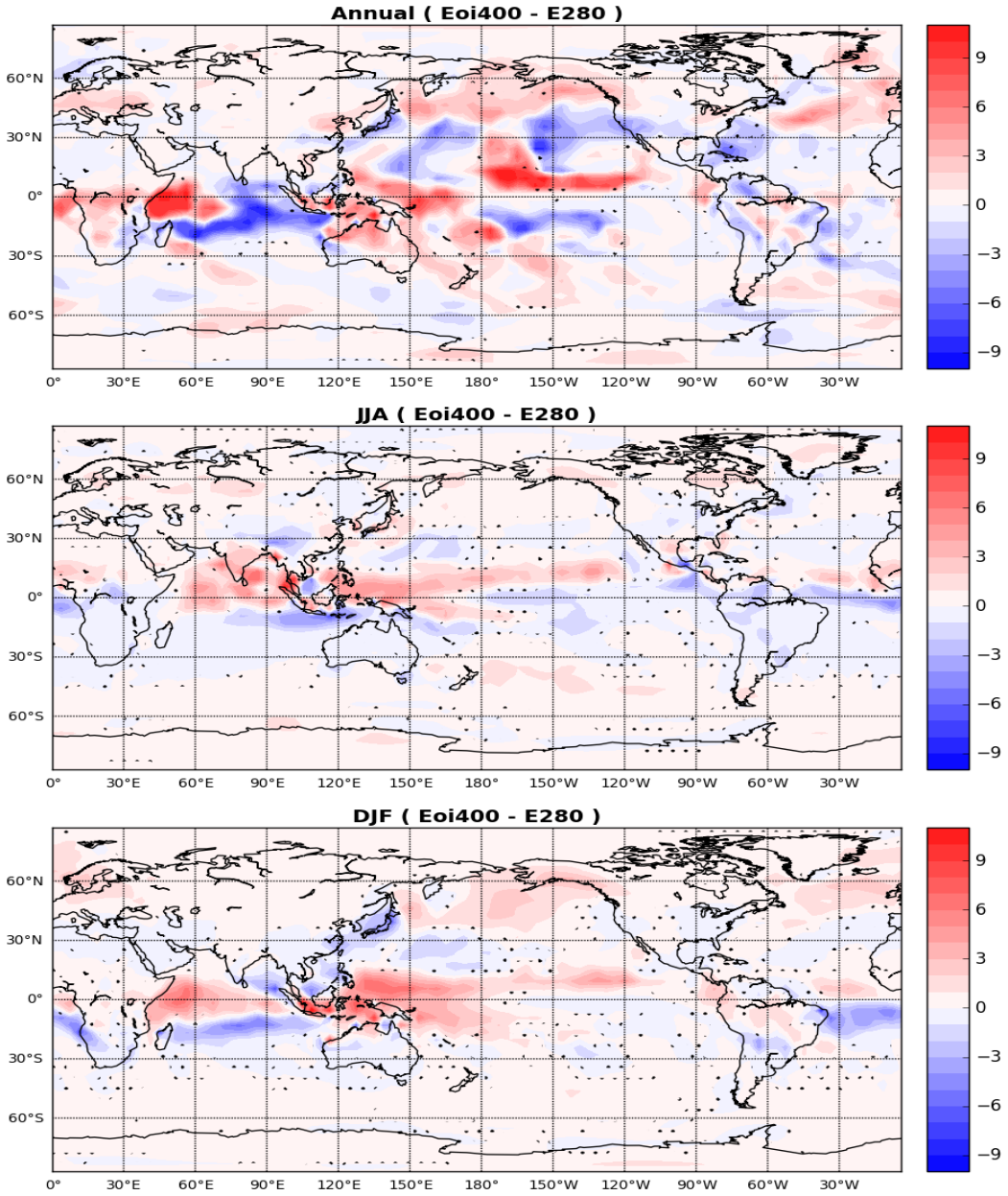

Figure 4.6: Anomalies of precipitation in mm/day between mid-Pliocene (Eoi400) and PI-control (E280) simulations. Shown are annual mean (a), boreal summer season (JJA) (b), and boreal winter season (DJF) (c). Time averages have been calculated from a 100-year time series of model output. Stipples (black dots) show regions of statistically insignificant differences.

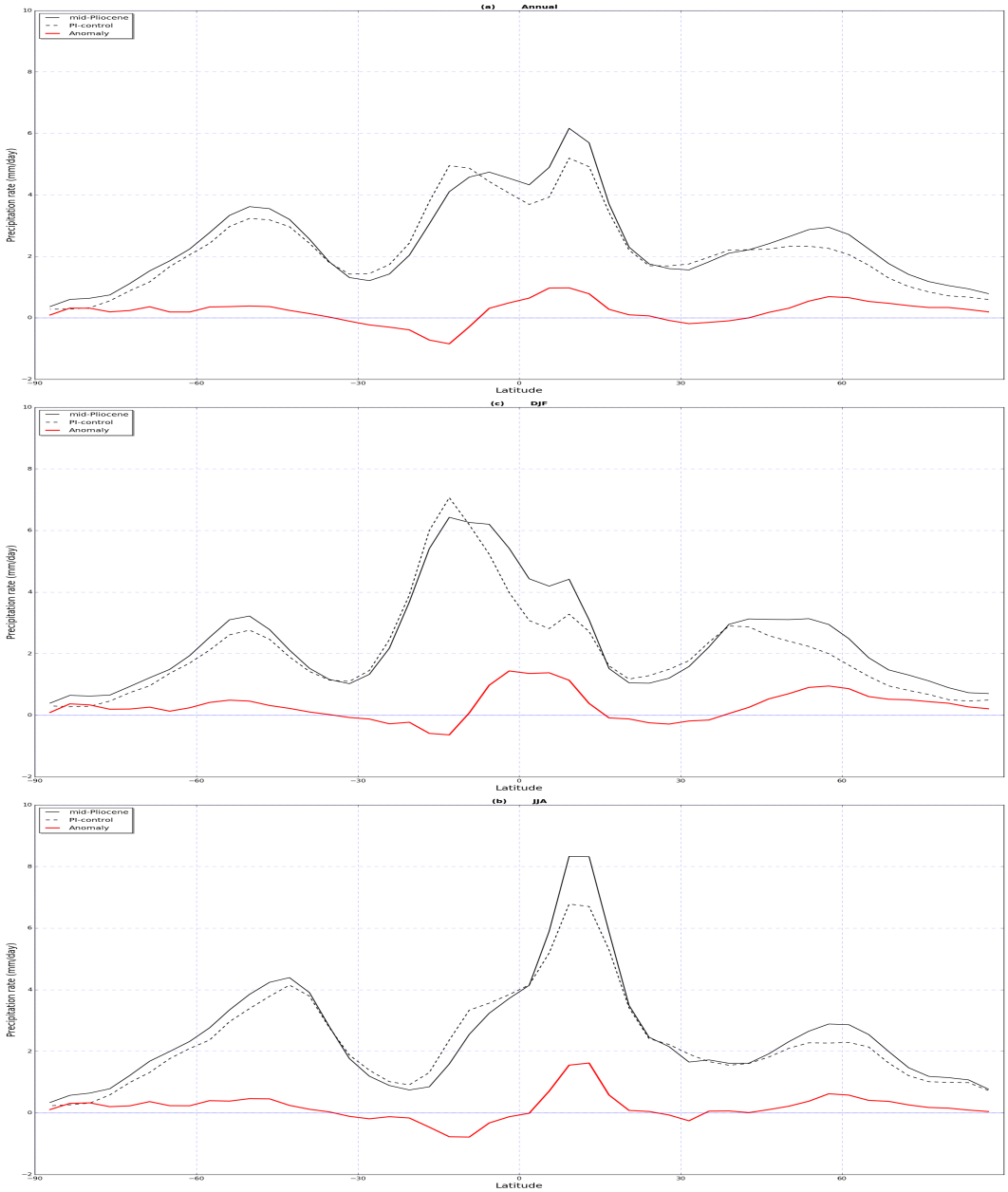

Figure 4.7: Annual (a), boreal summer (b) and boreal winter (c) zonal averages of precipitation. Time averages have been calculated from a 100-year time series of model output. The solid black line represent the mid-Pliocene while the dashed line denotes the PI-control conditions. Furthermore, the red line represents of the anomaly between mid-Pliocene and PI-control.

4.2.4 Sea surface temperature (SST)

Ocean surface maps of absolute SSTs for PI-control (E280, Figure 4.8a) and mid-Pliocene (Eoi400, Figure 4.8b) simulations show an equatorial warm pool in all the ocean basins of the world. This warm pool is the presence of warm water in the upper ocean around the equator, and characterized as regions where absolute SST values exceed 28°C (Watanabe, 2008). It extends in spatial extent in the mid-Pliocene simulation, which is a similar result to those obtained from COSMOS simulations for the first phase of PlioMIP as reported by Stepanek and Lohmann (2012). In the North and South Pacific, SST values are not only elevated, but also have increased spatial extent. The polar regions is relatively colder in comparison to the mid-latitude, and gradually heats up towards the equator.
A plot of the SST anomalies (Figure 4.8c) between the mid-Pliocene and PI-control simulations show increased temperature over the mid-Pliocene ocean, with few exception of local cooling. In the Pacific Ocean, cooling is observed along the eastern coast of Eurasia, with the most intense cooling is being present along the coast of Australia with a relative temperature drop of about -4.7 K. Furthermore, in regions close to the Antarctic, cooling with the most pronounced spatial extent is evident; this may be partly due to differences in the land-sea mask between the two simulations. On the other hand, substantial surface ocean warming occurs in the Northern Pacific as well as the Northern Atlantic. It is more pronounced in the former than the latter in terms of intensity and spatial extent.

4.2.5 Sea surface salinity (SSS)

Maps of sea surface salinity for PI-control (E280, Figure 4.9a) and mid-Pliocene (Eoi400, Figure 4.9b) as simulated by COSMOS, show that both simulations are characterized by high salinity in the Atlantic Ocean, Pacific ocean, Indian Ocean and also in the Mediterranean Sea which is a reasonable reproduction of the modern oceanography. More saline surface water is contained in the Atlantic Ocean, most especially in the mid-latitude regions where pronounced evaporation occurs, the Red Sea and the Mediterranean Sea. In comparison, the Baltic Sea, the North Pacific Ocean and the Arctic Ocean contain relatively fresher water.

Changes in SSS from the PI-control to the mid-Pliocene simulations (Figure 4.9c), show that the Arctic Ocean and large parts of the Pacific and Indian Ocean freshen, while the Atlantic Ocean becomes more saline. An exception to the general pattern of increased salinity gradient in the mid-Pliocene is the region of Western North Pacific Ocean, where salinity increases at an amplitude that is comparable to patterns found in most locations in the Atlantic Ocean. Ocean surface water along the eastern coast of Canada experience the most notable increase in salinity while the increased salinity along the coast of Malaysia is due to difference in land-sea mask in this region (compare Figure 4.9a and 4.9b).

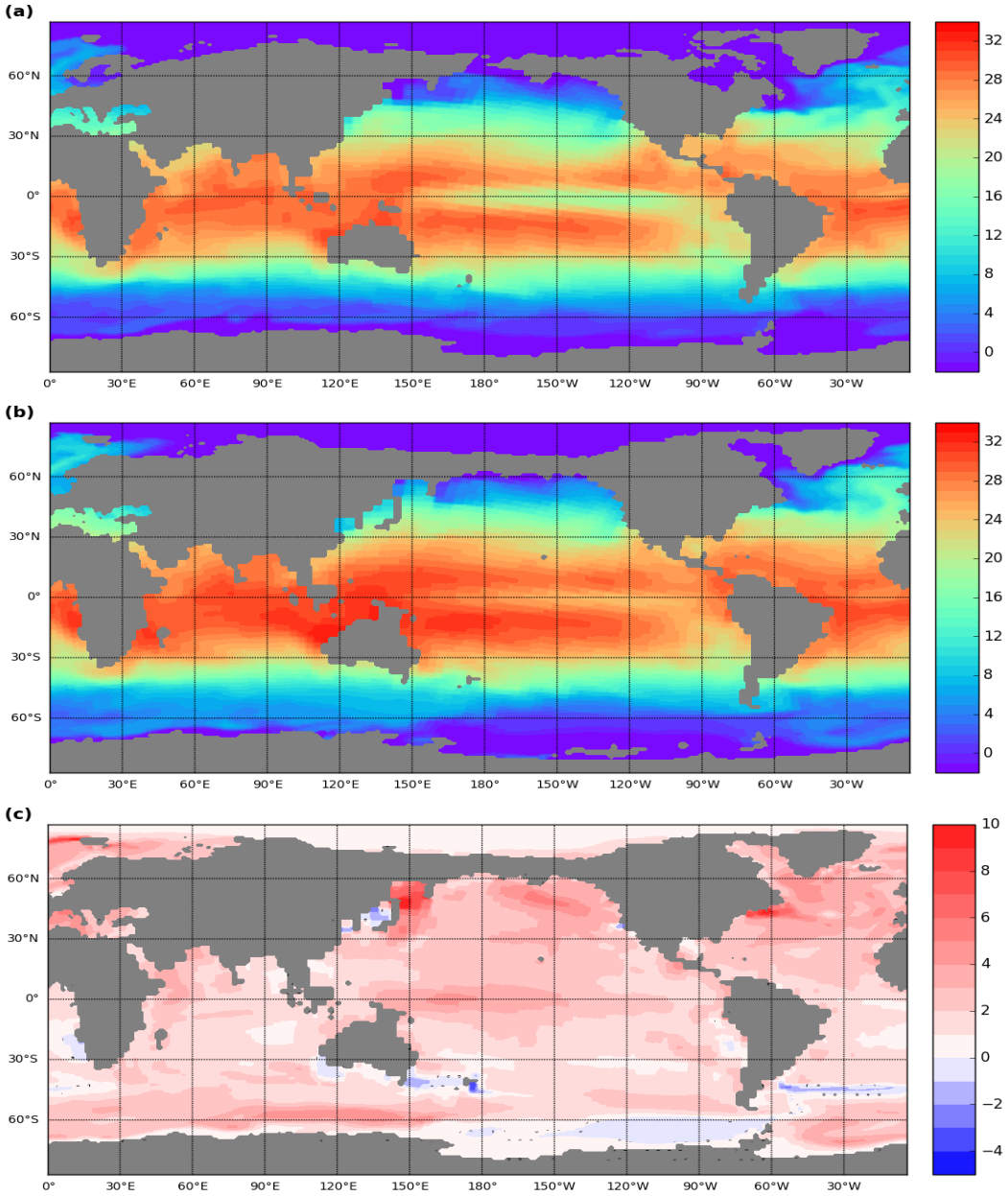

Figure 4.8: Annual mean sea surface temperature (°C), calculated from a 100-year time series of model output that has been interpolated from the curvilinear grid of the Ocean model to 1° x 1° grid. Shown are the PI-control (E280) simulation (a), the mid-Pliocene (Eoi400) simulation (b), as well as the anomaly between mid-Pliocene and PI-control (c). Stipples (black dots) show area of statistically insignificant differences

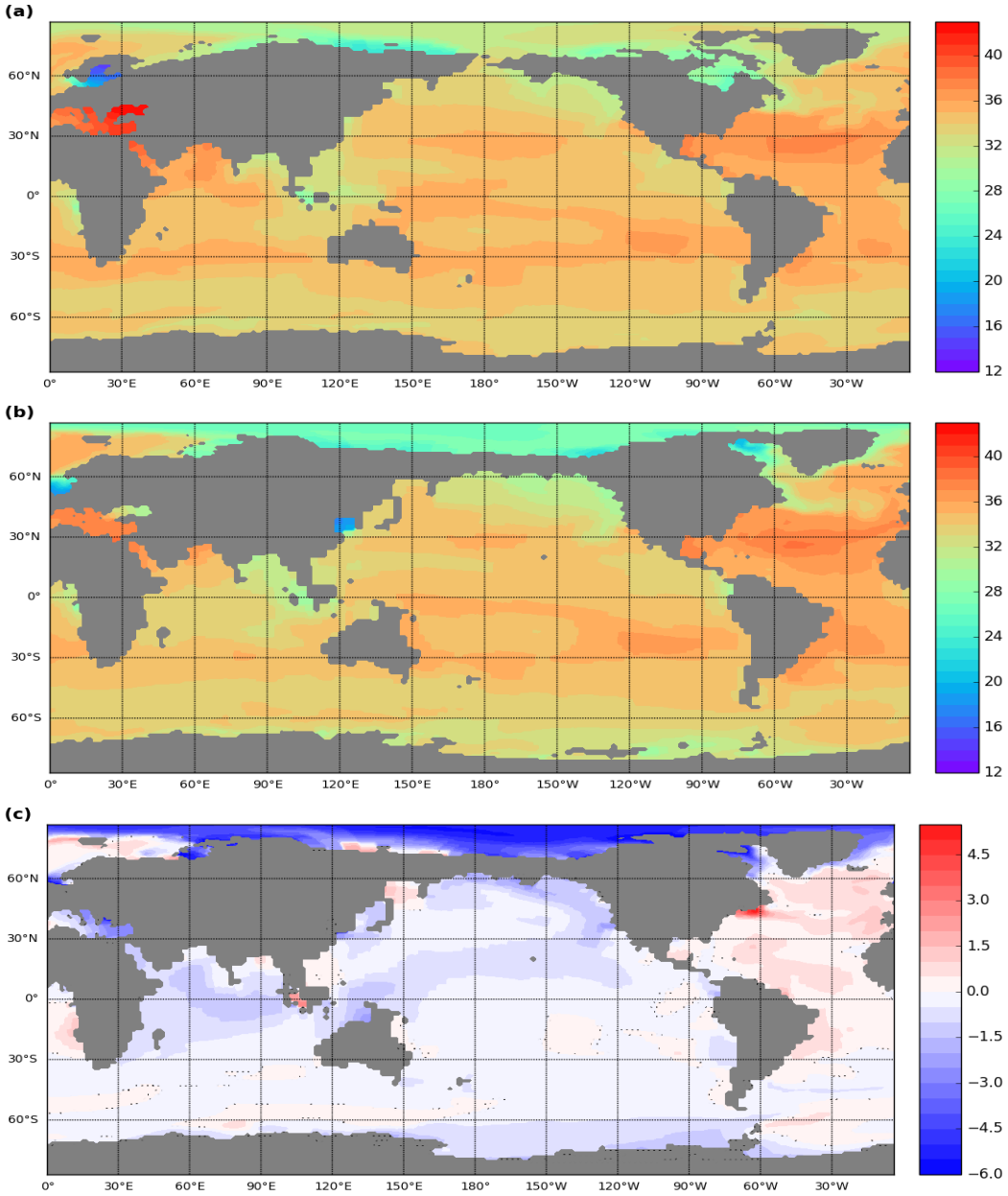

Figure 4.9: Annual mean sea surface salinity in PSU, calculated from a 100-yr climatology that has been interpolated from the curvilinear grid of the Ocean model to 1° x 1° grid. Shown are the PI-control (E280) simulation (a), the mid-Pliocene (Eoi400) simulation (b), as well as the anomaly between mid-Pliocene and PI-control (c). Stipples (black dots) show area of statistically insignificant differences

4.2.6 Atlantic Meridional Overturning Circulation (AMOC)

In general, COSMOS simulates a similar structure of the Atlantic meridional overturning circulation (AMOC) for the mid-Pliocene (Eoi400) and PI-control (E280) runs. However, there are few noticeable differences including the strength of the stream-function at different depths and the inflow of deep water from the south. According to results of the simulations, a maximum value of the meridional overturning stream-function of 18 Sv is present in the PI-control run while a maximum of 21.60 Sv is obtained for the mid-Pliocene simulation. Furthermore, in the mid-Pliocene simulation, the inflow of deep water from the South Atlantic, more precisely the strength of the Antarctic bottom water is decreased with respect to the PI-control simulation (compare Figure 4.10a and 4.10b). The meridional overturning circulation at depths shallower than 3000 m is slightly enhanced from PI-control to mid-Pliocene.

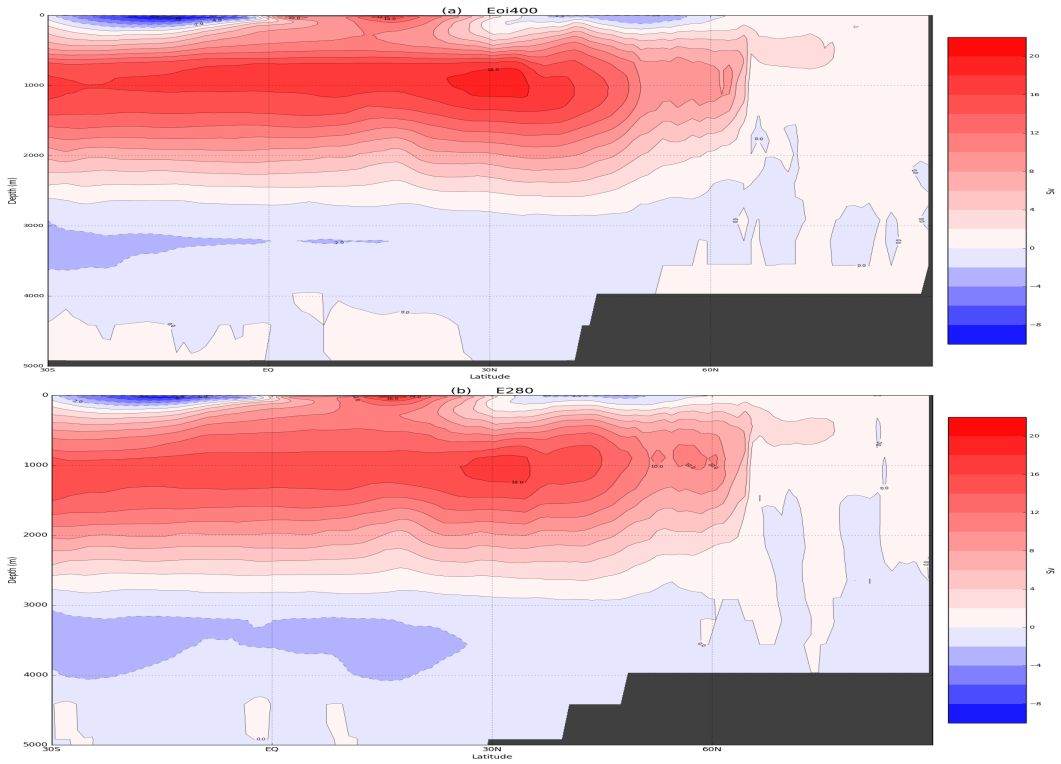

Figure 4.10: Comparison between simulated AMOC for mid-Pliocene and PI-control Atlantic Meridional Overturning Circulation (AMOC) in Sv for mid-Pliocene (a) and PI-control (b) simulations. Overturning rates are time averages that have been calculated from 100-year time series of model output. Positive values represent a clockwise circulation.

4.3 Comparison between COSMOS simulations for PlioMIP1 and PlioMIP2

4.3.1 Atmospheric quantities

The setups of mid-Pliocene simulations for PlioMIP1 and PlioMIP2 differs in ocean gateways, vegetation, prescribed palaeogeography and also in the concentration of CO_2. The prescribed concentration for the former is 405 ppmv and 400 ppmv in the latter. According to the simulation results, PlioMIP1's mid-Pliocene climate is about 2 K warmer than in PlioMIP2. COSMOS simulates similar patterns of mid-Pliocene SAT in response to PlioMIP's prescribed boundary conditions for PlioMIP1 and PlioMIP2, but there are few noticeable differences. The most pronounced annual average warming occurs in Polar regions. Generally, both mid-Pliocene simulations suggest land masses that are warmer than the ocean and increased Polar amplification, the latter is more pronounced in PlioMIP1 simulation (compare Figure 4.11a and b).

Due to changes in albedo and orography over Greenland and Antarctica, Greenland shows intense warming for both simulations, but the effect is more pronounced for the PlioMIP2 simulation. For the PlioMIP1 simulation, a warming of about 15 K is found over Greenland while the value is about 21 K for the second phase of PlioMIP.

Over Antarctica, there is strong temperature anomalies vary from one location to the other. In the South Pacific, rapid cooling is evident between 60°S - 70°S, extending from 65°W - 150°W for both simulations. This South Pacific cooling is about -1.2 K on the average with respect to the PI-control simulation for PlioMIP1, while it is more intense for PlioMIP2 with about -4 K and a wider spatial extent. Southern part of the Indian ocean experienced intense warming extending from 60°E into the South Pacific. The anomalies vary from 25.25 K in PlioMIP1 to 23.1 K in PlioMIP2 for the adjacent Antarctic landmass. The South Atlantic also exhibits SAT variations with areas within 80°S - 90°S cooling by about -1 K and -6 K for PlioMIP1 and PlioMIP2, respectively. Annual mean surface warming over the Hudson Bay is simulated for PlioMIP1 while the temperature there is largely unchanged for PlioMIP2.

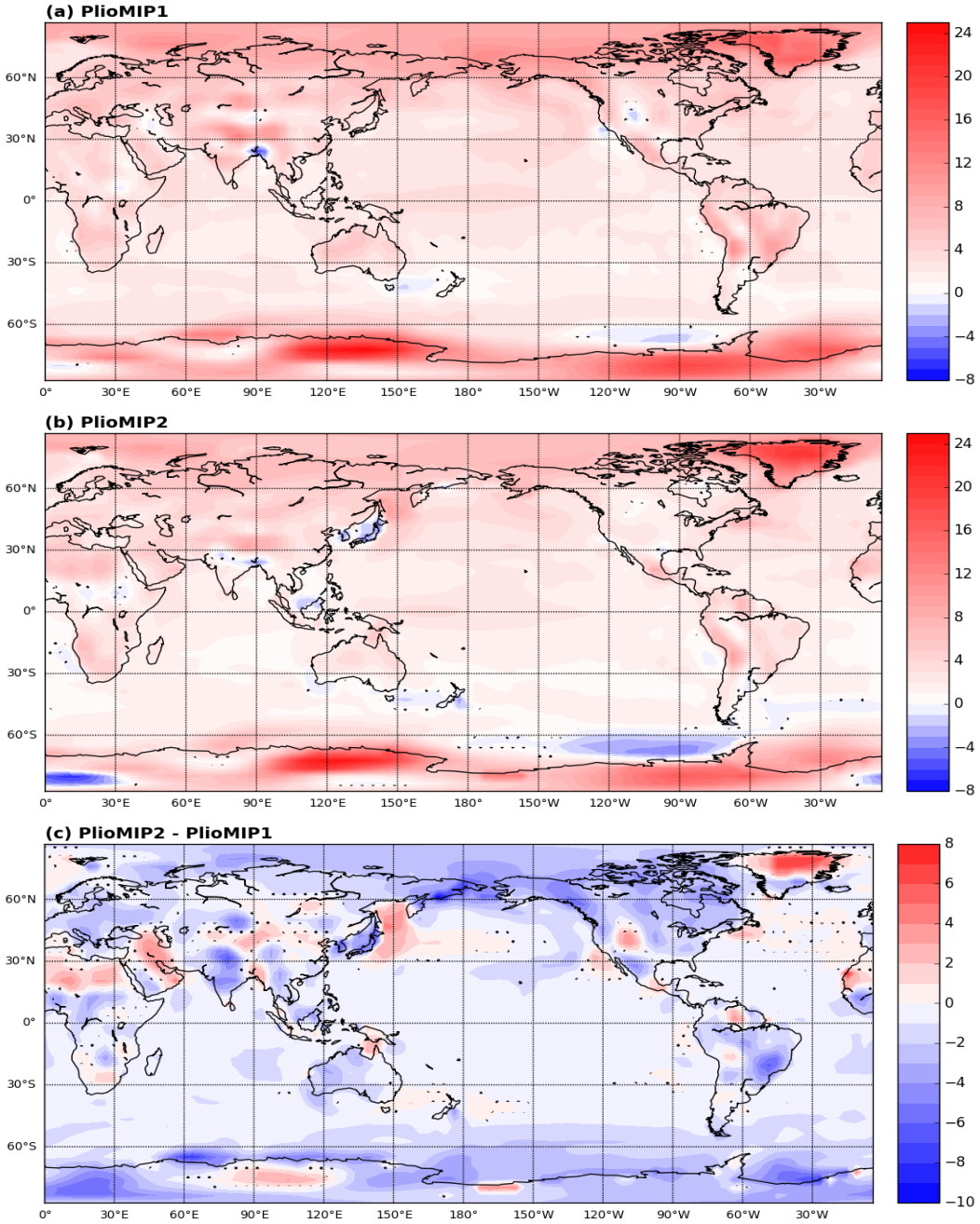

Figure 4.11: Comparison between mid-Pliocene simulated annual mean surface air temperature (SAT) in response to prescribed boundary conditions for PlioMIP1 (a) and PlioMIP2 (b) with respect to the PI-control simulation (E280), while (c) show the anomaly between PlioMIP2 and PlioMIP1 simulated SAT. Stipples (black dots) show area of statistically insignificant differences.

4.3.2 Oceanic quantities

Anomalies between simulated SST and PI-control for PlioMIP1 and PlioMIP2 show warming over the oceans (compare Figure 4.12a and b). Cooling is also observed over the oceans, but on a relatively small spatial extent. The cooling observed along the eastern coast of Eurasia in PlioMIP2 is absent in PlioMIP1 results from COSMOS. The cooling experienced along the coast of Australia is more pronounced in the PlioMIP2 simulation. SSS anomalies for PlioMIP1 and PlioMIP2 (see Figure 4.13a and b) show similar patterns in the Arctic and Atlantic Ocean. Contrary to the freshening found in the Pacific Ocean and Indian Ocean from PlioMIP2 simulation, PlioMIP1 results show that North Pacific Ocean becomes more saline as well as regions in the Northern Hemisphere of the Indian ocean.

AMOC obtained from the PlioMIP2 simulation show a stronger overturning circulation with respect to AMOC obtained from the PlioMIP1 simulation. According to results of both simulations, a maximum meridional overturning circulation of 20.5 Sv is obtained for PlioMIP1 while the corresponding value is 21.60 Sv for PlioMIP2. The inflow of Antarctic Bottom Water is more rapid for PlioMIP1.

Sea-ice seasons utilized in this study are as previously defined. Figure 4.5a, c and e refer to annual, winter and summer sea ice for PlioMIP2 while Figure 4.15a, b and c show the same for PlioMIP1. Comparison between simulated sea-ice for PlioMIP1 and PlioMIP2 show that the Canadian Arctic Archipelago is totally free of sea ice for PlioMIP2 simulation while PlioMIP1 results show considerable sea ice over the region. In the annual mean, the simulated sea ice is gradually reduced from the pole towards the coastlines for both PlioMIP1 and PlioMIP2. Both simulations show that the mid-Pliocene ocean is ice-free during summer based on the definition of sea ice summer adopted for this study, with sea ice compactness less than 15% (Figure 4.5c and Figure 4.15c).

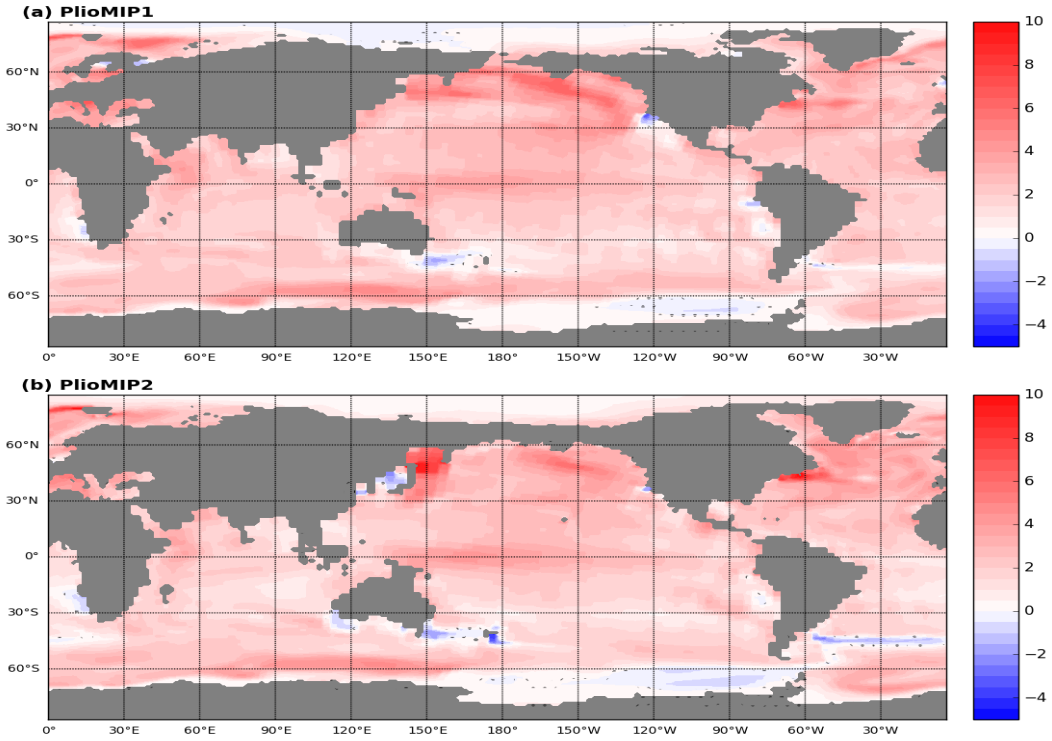

Figure 4.12: Comparison of mid-Pliocene sea surface temperature (°C) anomalies calculated from 100 years of model output, with respect to PI-control simulation as obtained from COSMOS for the two phases of PlioMIP, namely PlioMIP1 (a) and PlioMIP2 (b).

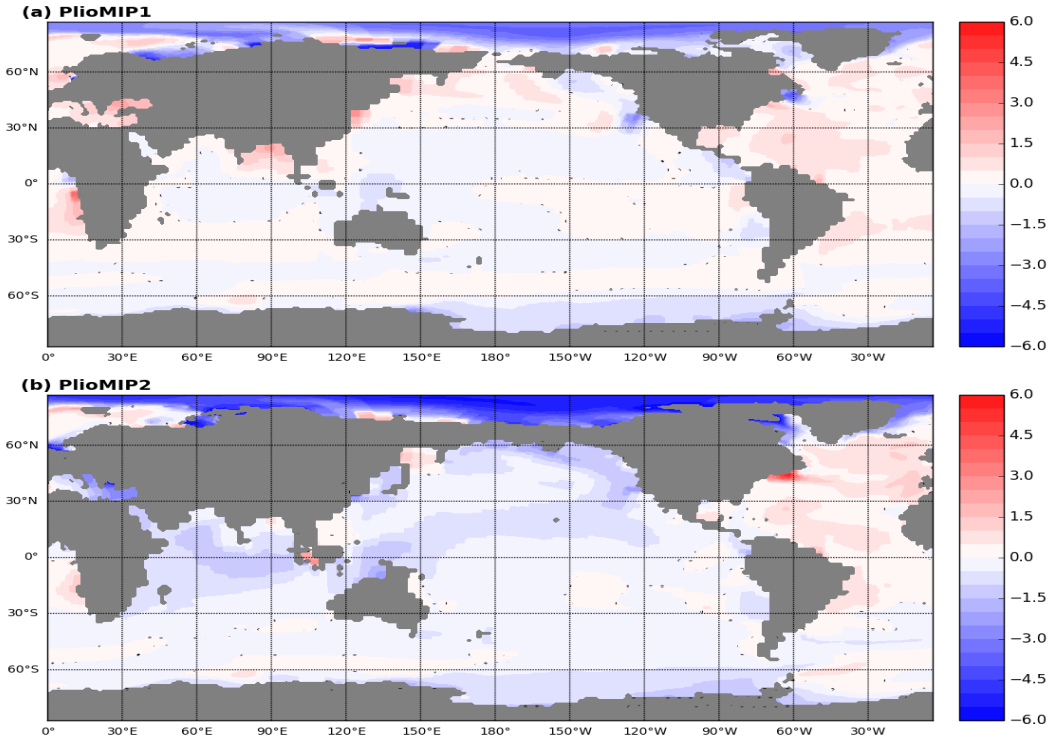

Figure 4.13: Same as Figure 4.12, but for sea surface salinity (PSU)

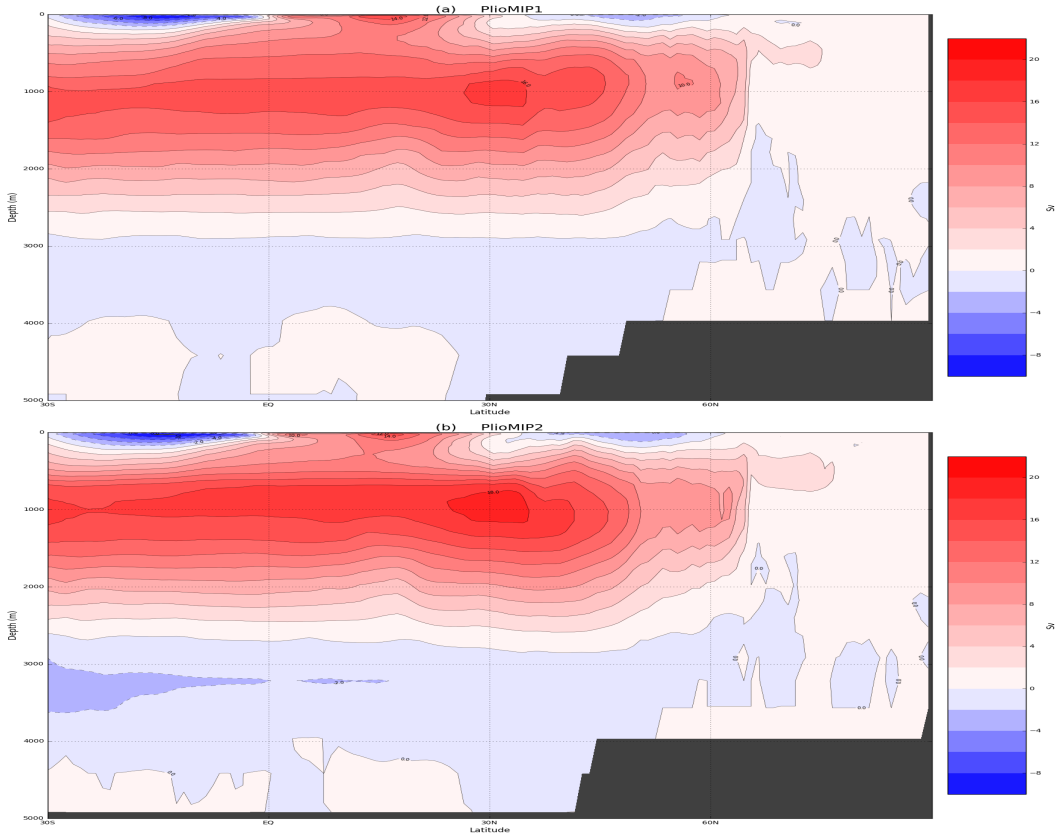

Figure 4.14: COSMOS simulated mid-Pliocene annual mean AMOC in Sv for PlioMIP1 (a) and PlioMIP2 (b). Overturning rates are time averages that have been calculated from 100-year of model outputs. Positive values represent a clockwise circulation.

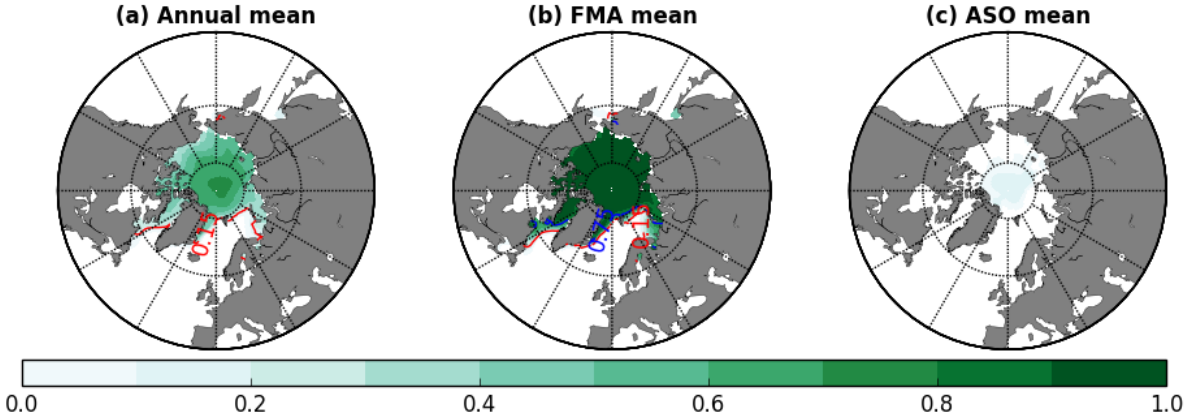

Figure 4.15: Annual and seasonal mean mid-Pliocene sea ice compactness over 100 model year as simulated by COSMOS for PlioMIP1. (a), (b) and (c) show the annual, winter (FMA) and summer (ASO) averages.The red contours indicate 15% isoline of sea ice cover while blue contours indicate 75% isoline of sea ice cover. Missing data at the pole is a plotting artifact.

4.4 Data-model comparison of SST

4.4.1 Effect of Bering Strait closure on the agreement of simulated North-Atlantic SST with its reconstruction

PlioMIP1 model ensemble show a persistent underestimation of the reconstructed North Atlantic SST (Dowsett et al., 2013), and the COSMOS is not an exception in this respect. A closed Bering Strait has been said to increase the AMOC, which in turn provides an increased ocean heat transport to the North Atlantic, leading to warmer SSTs in the North Atlantic (Hu et al., 2015; Otto-Bliesner et al., 2017).

In this study, simulated COSMOS PlioMIP1 (with open Bering Strait) SSTs are compared with PlioMIP2 (with closed Bering Strait) results simulated with the same model. The AMOC simulated in the PlioMIP2 simulation is stronger than its PlioMIP1 counterpart (Figure 4.14), leading to a relative warming of 2 to 4 °C in the North Atlantic. This warming indicates an improved level of agreement between PlioMIP2 simulated SSTs and the reconstruction.

However, the underestimation noticed in the PlioMIP1 simulations of Stepanek and Lohmann (2012) is also present in PlioMIP2 simulations even with a closed Bering Strait, but with relatively increased agreement in comparison to PlioMIP1 simulated North Atlantic SSTs. RMSE of 2.60 is evident for the simulated PlioMIP1 SSTs with respect to PRISM3 SST reconstruction of (Dowsett et al., 2009). A corresponding value of 2.21 is present for the PlioMIP2 simulation of SST by COSMOS. In conclusion, agreement between simulated North Atlantic SSTs with reconstruction of the mid-Pliocene is better if the Bering Strait is closed.

Furthermore, the Bering Strait is only one contributor to the better agreement found between PlioMIP2 SSTs and its reconstruction. There are other changes in the boundary conditions between PlioMIP1 and PlioMIP2, including some gateway changes that have similar effect as the Bering Strait (Otto-Bliesner et al., 2016).

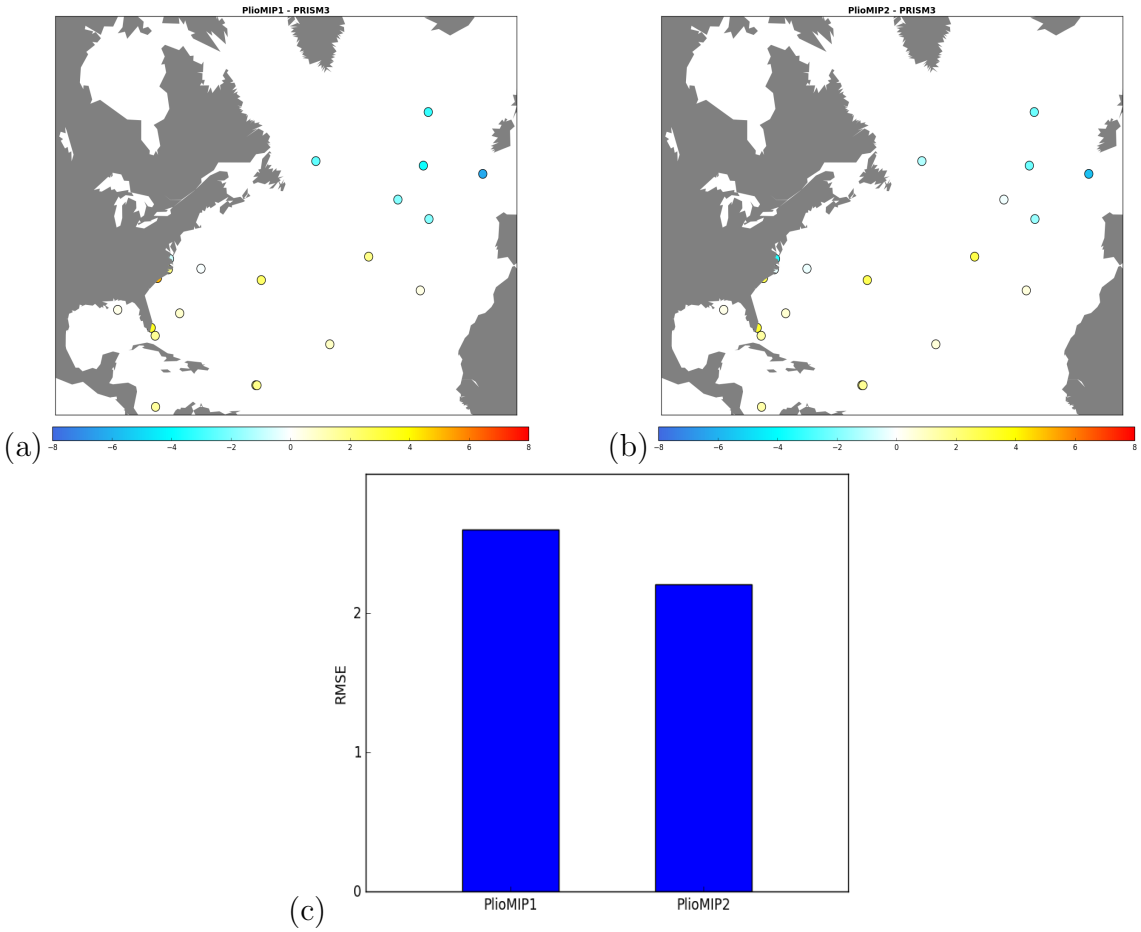

Figure 4.16: Differences between mid-Pliocene sea surface temperature (SST) anomaly (K) and the reconstruction of Dowsett et al. 2013. (a) show the biases between COSMOS simulated SSTs for PlioMIP1 (with open Bering Strait) and the reconstruction, while (b) show the same as (a) but for PlioMIP2 (with closed Bering Strait). (c) show the RMSE with respect to COSMOS simulations for PlioMIP1 and PlioMIP2.

4.4.2 Could uncertainty in the level of atmospheric CO_2 be the reason for model-data mismatches?

Even with the closure of the Bering Strait, mid-Pliocene SSTs are not totally in agreement with the reconstruction. A further step is taken to ascertain if the concentration of atmospheric CO_2 specified for the simulations plays a role in the disagreement. Data-model discord, especially the disagreement of simulated mid-Pliocene SST with its reconstruction is quantified for different simulations with mid-Pliocene geography and varying concentration of atmospheric CO_2 namely, 350, 400 and 560 ppmv. The result show that the uncertainty in the concentration of atmospheric CO_2 specified for the mid-Pliocene simulation could contribute to the high level of data-model mismatch. Eighteen different regions of the Oceans are classified and named according to their location as described in Table 4.2.

In the regions NNP, NWA, MS, EqP, EqA, EqWP, I and NA (see Figure 4.18), Eoi350

Table 4.2: Classification of ocean regions defined for regional comparison of simulated SSTs with the reconstrution.

Abbreviation	Location	Abbreviation	Location
haNA	high amplitude North Atlantic	NWP	North-West Pacific
NNP	North-North Pacific	SEP	South-East Pacific
haAr	high amplitude Arctic	SP	South Pacific
SA	South-Atlantic	EqA	Equatorial Atlantic
I	Indian	SO	Southern Ocean
NWA	North-West Atlantic	EqWP	Equatorial-West Pacific
EqP	Equatorial-Pacific	Ar	Arctic
MS	Mediterannian-Sea	NP	North-Pacific
NEP	North-East Pacific	NA	North-Atlantic

provides the best agreement with the SST reconstruction of Dowsett et al. (2009). The equatorial warm pool present in simulations with higher CO_2 concentration is also present, but with a reduced spatial extent. The low-latitude warming present in Eoi400 and Eoi560 is not supported by the reconstruction. According to the RMSE analysis, Eoi400 gives the best fit with the reconstruction in the SA, NWP, SP, SO and the NP, while the Eoi560

is in a better agreement with mid-Pliocene SST reconstruction in the haNA, haAr, NEP and SEP. The Arctic Ocean SST gives the same value of RMSE for the three simulations. This is attributed to the land-sea mask utilized in the simulation of mid-Pliocene climate, where the location of the Arctic reconstruction is represented as land in the simulations. On the global scale, simulation Eoi400 gives the lowest value of RMSE, showing that the model-data is on the minimal with CO_2 concentration of 400 ppmv . The overall best agreement is in the NP with a RMSE of 0.2 in the Eoi400 simulation. The Eoi560 also recorded a relatively good fit with the RMSE of 0.48. It is however noted that the reconstruction of SST at the location was carried out for a single point which may not be a true representative of the actual mid-Pliocene SST in this region.

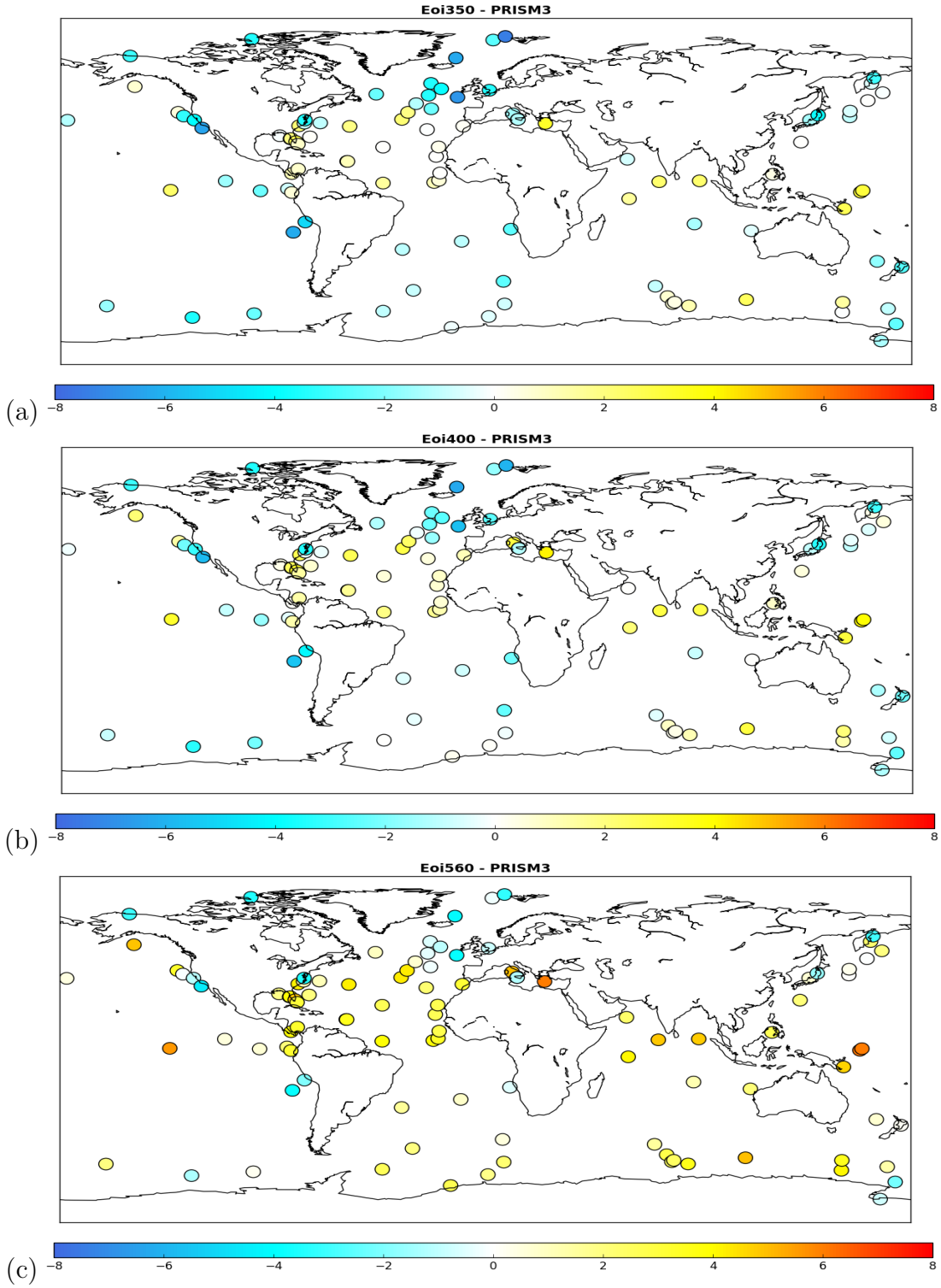

Figure 4.17: Sea surface temperature (SST) anomalies (K) in PlioMIP2 mid-Pliocene runs with respect to PRISM3 proxy-based SST reconstruction of Dowsett et al. (2009). (a), (b) and (c) show the anomalies mid-Pliocene simulations Eoi350, Eoi400 and Eoi560, respectively, with respect to the reconstruction.

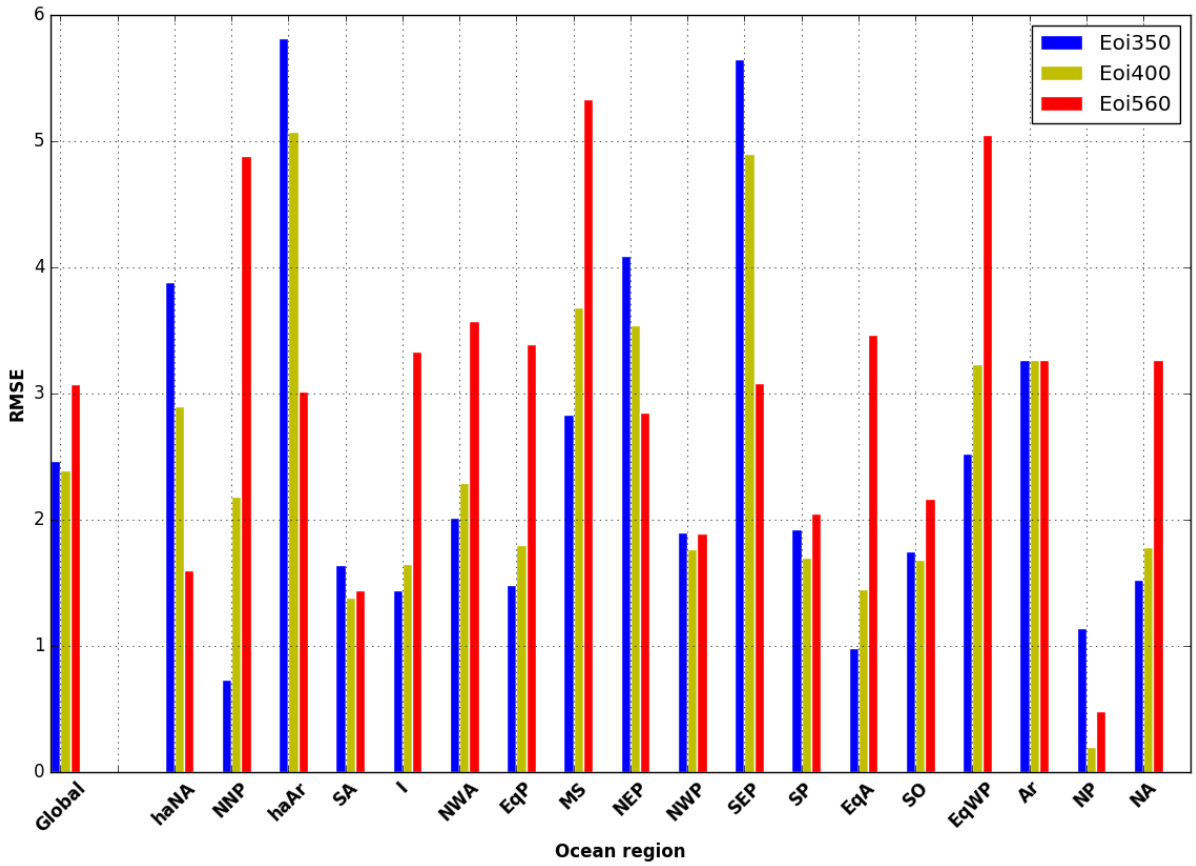

Figure 4.18: Root mean square error (RMSE) of simulated mid-Pliocene sea surface temperature (SST) for different regions of the ocean with the reconstruction of Dowsett et al. (2009). Blue bars indicates the RMSE calculated from mid-Pliocene simulation with atmospheric CO_2 level of 350 ppmv with respect to PRISM3 SST reconstruction, while the green and the red bar represent the RMSE calculated with mid-Pliocene simulations with atmospheric CO_2 concentration of 400 and 560 ppmv, respectively.

4.5 Climate oscillation in COSMOS simulations under high CO_2 forcing

Generally, the amplitude of oscillation in COSMOS outputs varies between considered simulations. Simulations E400, E560 and E600 (see description in Table 3.1) are considered in the analyses. The oscillation under the influence of high atmospheric CO_2 is analysed by classifying the model output into 3 different phases, that are characterized by the relative temperature namely warm, cold and intermediate. The selected years, that represent a typical phase of the oscillating climate in this analysis, are given in Table 4.3.

Table 4.3: Selected years of the modelled time-series of sea surface temperature utilized in the analyses of different phases of the oscillation.

Simulation	Warm	Intermediate	Cold
E400	5400 - 5499	4250 - 4349	6200 - 6299
E560	3000 - 3099	4310 - 4409	5400 - 5499
E600	3000 - 3099	4640 - 4739	4500 - 4599

Considering SST anomalies for different phases of the oscillations in the Southern Ocean increased warming from the cold to the warm phase is observed with localized cooling also present around the Ross Sea. The warming intensifies and increases in spatial extent with increasing CO_2, extending from the Southern Ocean to 45°S in E400 and up to the equator in the E560 simulation. This surface warming extends into the Northern Hemisphere in the E600 simulation. Globally, most regions depict positive SST anomalies, while negative anomalies are seen in the Ross Sea, the North Pacific and North Atlantic. Apart from the cooling of the Ross Sea, the pattern of changes between warm and cold phases is consistent with the model-data comparison of Latif et al. (2013), with respect to oscillation in the Southern Ocean.

This study show that the change of Ocean temperature with depth is more pronounced in the E560 and E600 simulations than the E400. In the Atlantic, simulation E400 shows a warm ocean surface anomaly between the warm and the cold phase, with mid-ocean

cooling from about 1000 m to the deep ocean(see Figure 4.22). Simulations E560 and E600 show similar pattern in the Atlantic with the transport of Southern Ocean surface warm water pronounced throughout the different depths of the basin. The warming is more intense at the surface with a temperature change of +1.6 K between warm and cold phases. A gradual cooling is noticed as it mixes downward. There is an inflow of extended Antarctic bottom water into the Atlantic as well as the North Atlantic deep water. Anomalies between the warm and the intermediate phases show a different pattern to the warm-cold anomalies for E560, while E600 show similar pattern. The mid Ocean cooling in the warm - cold analysis of E560 and E600 is absent for the warm-intermediate analysis. In contrast, simulation E400 shows cooling of the surface ocean in the equatorial region, and warming in the deep ocean with the exception of the Polar regions. The anomalies between the intermediate and cold phases show different patterns, with surface warming pronounced across all the 3 simulations. Mid-depth ocean cooling is found in simulations E400 and E560, while warming is dominant in simulation E600. Similar patterns of Intermediate - cold phases is found in all the Indian, as well as the Pacific Ocean.

Furthermore in the Pacific, surface ocean warming is recorded in all the considered simulations with an exception in the North Pacific for simulation E600, where cooling is observed. Bottom water cooling is witnessed between the warm and cold phases as well as the warm and intermediate phases for E560 and E600. The warm - cold anomalies show a different pattern from the warm - intermediate anomalies where warming of the bottom water is eminent. The Indian Ocean accommodates more heat as the pattern of changes in Ocean temperatures is different in comparison to the Atlantic and the Pacific. Warming is pronounced throughout the ocean with the exception of the Antarctic Bottom water sources in the Indian Ocean, where cooling is recorded.

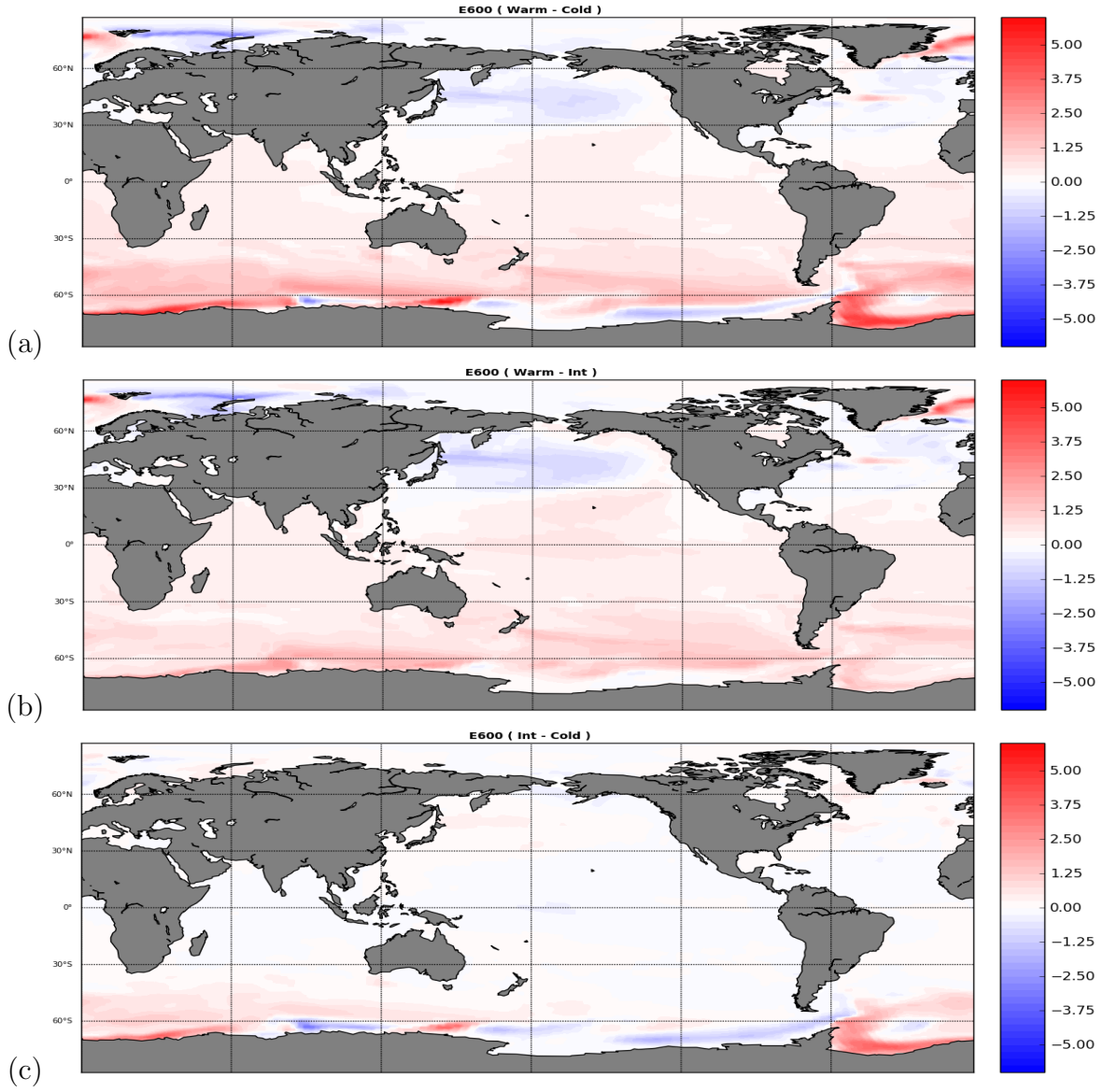

Figure 4.19: Simulated sea surface temperature anomalies between (a) warm and cold, (b) warm and intermediate and (c) Intermediate - cold phases of the oscillatory regime of the simulation with high CO_2 and modern geography .

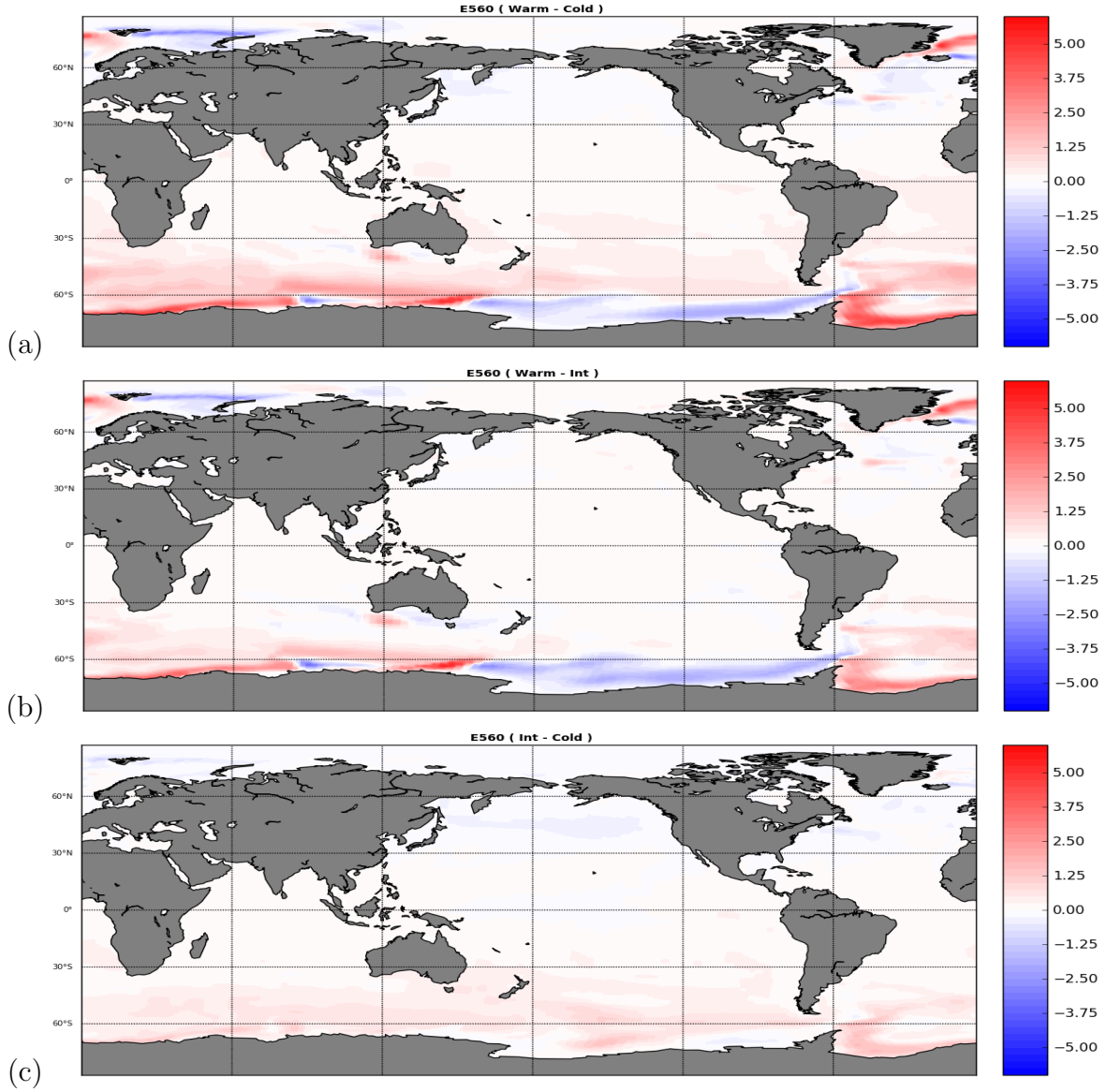

Figure 4.20: Same as figure 4.19, but for simulation E560, which implies a simulation with atmospheric CO_2 of 560 ppmv.

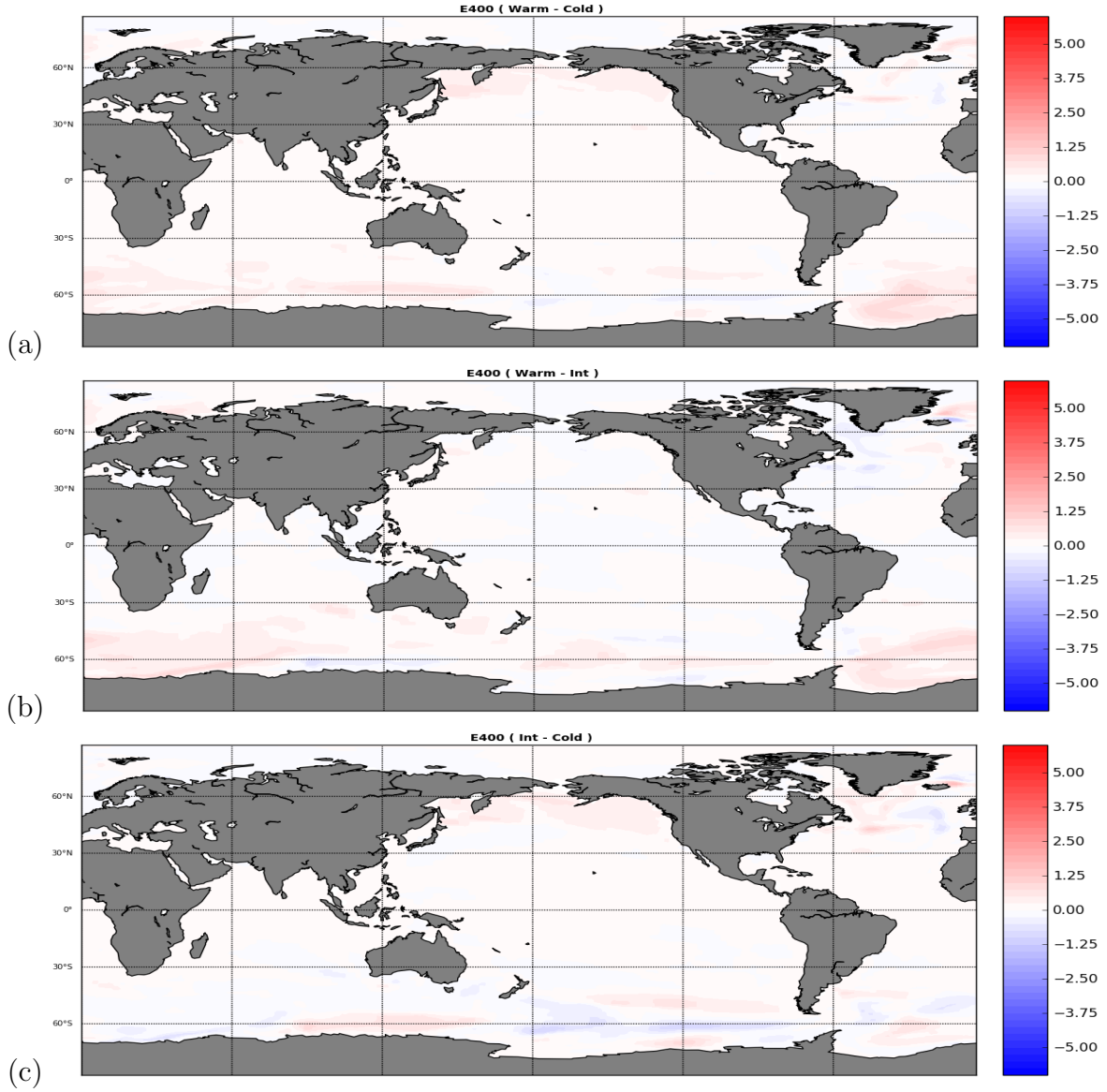

Figure 4.21: Same as figure 4.19, but for simulation E400, which implies simulation with atmospheric CO_2 of 400 ppmv.

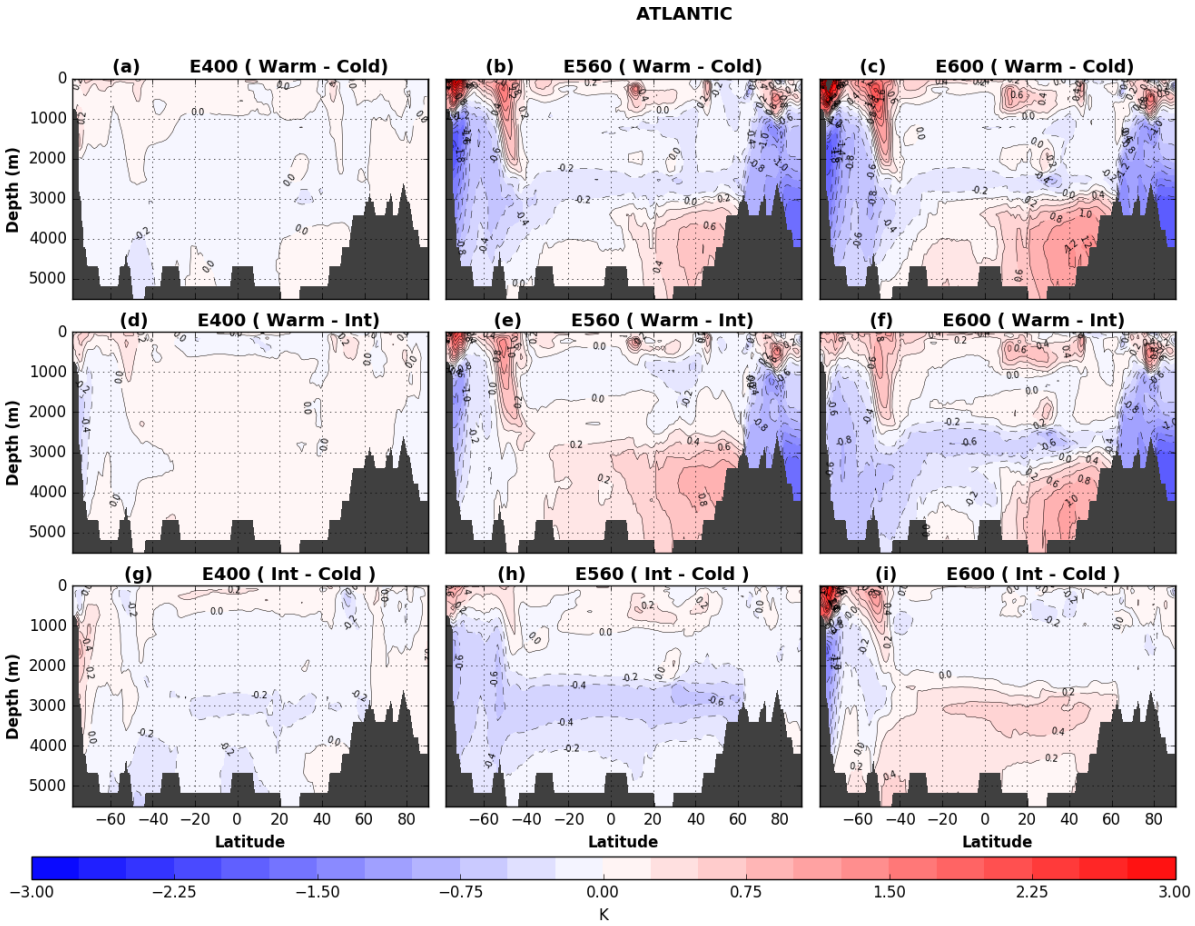

Figure 4.22: Ocean temperature anomalies between different phases of oscillation in the Atlantic ocean. (a),(d) and (g) show for simulation E400, the anomalies between warm and cold, warm and intermediate and between intermediate and cold, respectively. (b), (e) and (f) show in the same sequence as described for E400, but for simulation E560. For E600, warm - cold (c), warm - intermediate (f) and intermediate - cold (i).

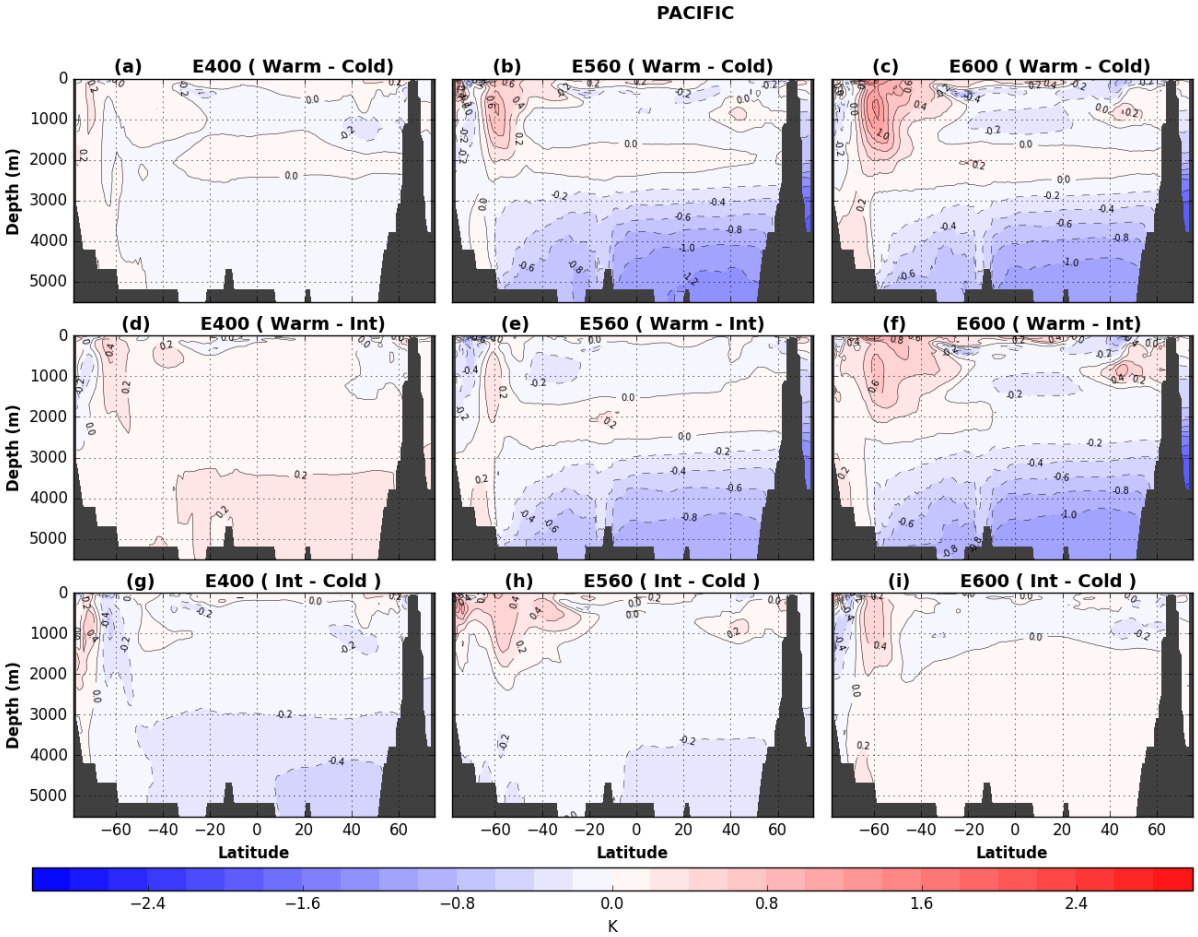

Figure 4.23: Same as in Figure 4.22, but for the Pacific Ocean.

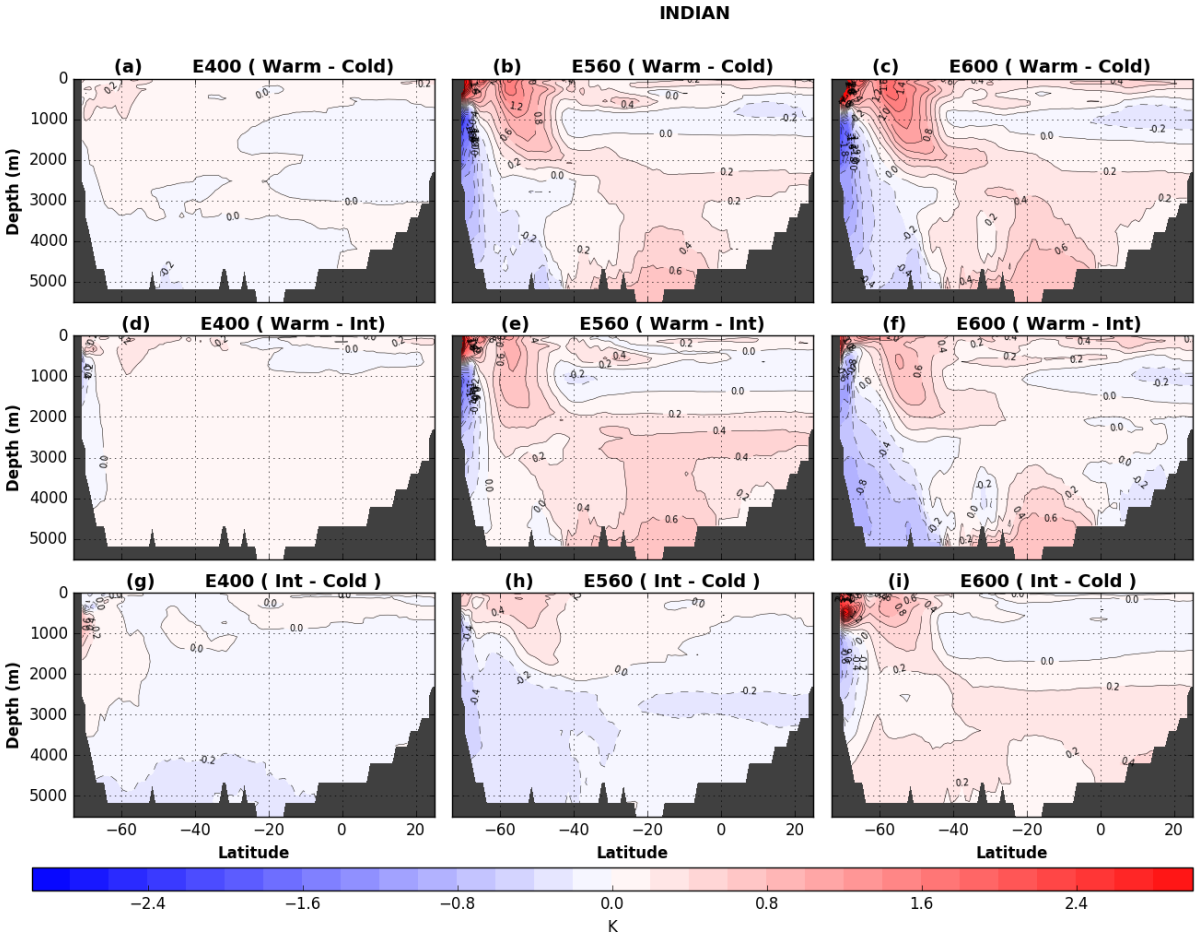

Figure 4.24: Same as in Figure 4.22, but for the Indian Ocean.

CHAPTER 5

Discussion

In this chapter, a discussion of CS response to different background geographies is presented. Analyses of the mid-Pliocene experimental results for PlioMIP2 as simulated by COSMOS, as well as comparison of PlioMIP1 and PlioMIP2 results are also discussed. Furthermore, evaluation of simulated SSTs in comparison with its proxy based reconstruction are discussed. The discussion concludes with an assessment of results obtained for climate oscillation under high CO_2.

5.1 State-dependence of climate sensitivity

The COSMOS CS has been estimated and compared for two different climate states. It is found that the estimates differ between PI and the mid-Pliocene as simulated by COSMOS. Studies have revealed that the sensitivity of Earth's surface air temperature to radiative forcing is on the average warming of 3 K per doubling of atmospheric CO_2 concentration, and estimates with high confidence levels range from 1.5 to 4.5 K (Knutti et al., 2006; Pagani et al., 2010; Rohling et al., 2012; von der Heydt and Ashwin, 2016). CS estimates presented in this study fall within the specified range, with simulations with

mid-Pliocene geography suggesting a CS of 4.5 K while simulations with PI geography suggests a value of 4.2 K. The mid-Pliocene climate is characterized by increased SST from mid to high latitudes, reduced sea ice extent and thickness of ice sheets, a sea level rise of at least 25 m, and the presence of warmth or moisture loving vegetation at middle to high latitudes compared with the present (Dowsett et al., 1999). With the differences between both climate ensemble being the prescribed land ice and orography, a higher CS is expected for the mid-Pliocene than the PI climate. Loss of sea-ice, reduction of ice sheet thickness and area will result in less reflective earth surface, an effect known as the ice-albedo feedback, causing the earth to absorb increasing amount of shortwave radiation. An enhanced Arctic warming is present in the mid-Pliocene simulation, and of course a warmer SST than in its PI counterpart. Furthermore, warmer climates have been identified to be more sensitive to CO_2 forcings than colder climates (Friedrich et al., 2016; Heydt et al., 2014; Köhler et al., 2010). The results obtained from the comparison show a good agreement in this respect, as the simulated mid-Pliocene climate is warmer relative to the simulated PI climate. CS is dependent on the underlying climate state and the state of imposed boundary conditions (Hargreaves and Annan, 2016; Yoshimori et al., 2011).

Considering the common methodology of CS estimation in the climate modelling community, several uncertainties must be considered. Proxy-based reconstructions of past climates, which are available for comparison are uncertain. In the same direction, forcing uncertainty is a major issue in simulating past climates with the precise concentration of atmospheric CO_2, that is not available. The results presented here are not expected to provide a true value for the CS in the studied climate ensemble, but it is an indicative that CS is dependent on the background climate.

5.2 Effect of changes in mid-Pliocene boundary conditions on COSMOS outputs

One of the main objectives of PlioMIP is to determine the dominant components of mid-Pliocene warming derived from the imposed boundary conditions (Haywood et al., 2016). Global annual mean SAT estimated from PlioMIP model ensembles increased by 1.8 to 3.6 K (Haywood et al., 2013; Haywood et al., 2016). For the COSMOS simulation in response to PlioMIP1 boundary conditions, the most pronounced warming is recorded over areas where changes in albedo and orography have been implemented (Stepanek and Lohmann, 2012). This is also the case for PlioMIP2 simulation with the same model. However, the increased number of simulations with dedicated sensitivity studies in PlioMIP2 allows a proper inference of the main driver of mid-Pliocene warmth. This study found that the intense warming recorded in the Polar region is mainly due to increased CO_2 while mid-Pliocene orography and ocean gateways contributes more relative to the location where they are applied.

Furthermore, PlioMIP1 model ensemble showed enhanced mid-Pliocene AMOC which contributes to warming in the North Atlantic (Zhang et al., 2013). Zhang et al. (2013) stated further that the signal and strength of the meridional transport in the Atlantic vary from model-to-model, and none of the model ensemble were able to reproduce the substantial enhancement of the AMOC as implied by the proxy record (Raymo et al., 1996; Robinson, 2009). In an attempt to simulate enhanced AMOC, studies suggested that the closure of the Bering Strait would lead to enhanced AMOC (e.g. Hu et al., 2015) and also the prescription of sea floor topography could lead to an enhanced AMOC (Brierley and Fedorov, 2016; Motoi et al., n.d.; Robinson et al., 2011). With all these having been incorporated into PlioMIP2 experiments, COSMOS simulated an enhanced AMOC for PlioMIP2 with respect to its PlioMIP1 output.

Half of the PlioMIP1 model ensemble, in which COSMOS is part of, simulated sea ice free mid-Pliocene summer in the Arctic Ocean (Howell et al., 2016). This is consistent

with the result obtained from PlioMIP2 for COSMOS.

5.3 Data-model discords

Simulated SSTs in the framework of PlioMIP1 was underestimated in the North Atlantic with respect to the available mid-Pliocene SST reconstruction of Dowsett et al. (2009). In the same direction, mid-to-high-latitude SST warming was also underestimated among all PlioMIP1 model ensembles (Dowsett et al., 2013). COSMOS simulated mid-Pliocene SST for the first phase of PlioMIP is characterized by equatorial warm pool and low latitude warming, which differ greatly from the reconstruction (Stepanek and Lohmann, 2012). With the effect of ocean gateway changes being in the fore-front of discussions on mid-Pliocene data-model discrepancies, the true state of the Bering Strait during this time-slice is largely unknown (Gladenkov et al., 2002).

The Bering Strait first opened very near to the end of the Miocene at about 5.32 Ma BP (Gladenkov et al., 2002). It remains an uncertainty whether the Bering Strait is closed or opened during the mid-Pliocene. Hu et al. (2015) gave an overview of the influence of an opened or closed Bering Strait on simulation results regardless of the time-slice being studied. A closed Bering Strait results in the strengthening of the AMOC, which as a consequence leads to a warmer North Atlantic and a relatively cooler North Pacific.

Results obtained from COSMOS simulations for PlioMIP1 and PlioMIP2 were compared with the mid-Pliocene reconstruction of SST in the North Atlantic, with the Bering Strait opened in the former and closed in the latter. Based on a comparison using RMSE between reconstructed mid-Pliocene SST and COSMOS simulations for PlioMIP1 and 2, a closed Bering Strait leads to better agreement with the proxy-based reconstruction.

The importance of a closed Bering Strait in resolving data-model disagreement for the mid-Pliocene cannot be overemphasized, as it does not completely resolve the understimation of SST reconstruction. Varying mid-Pliocene CO_2 in different regions of the ocean show that the uncertainty in concentration of atmospheric CO_2 during the mid-Pliocene could also contribute to the discord.

5.4 Variability of Southern Ocean SSTs

Southern Ocean SSTs have been identified to exhibit centennial variability, and the existence of such centennial variability is supported by instrumental records (Latif et al., 2013). Furthermore, Kiel Climate Model has shown a similar pattern of the Southern Ocean Centennial Variability (SOCV) produced by the instrumental records (Latif et al., 2013). Until now, the variability is believed to be internally driven and independent of external forcings. Studies have shown that warming of Southern Ocean deep water and contraction of the Antarctic bottom water, occurs as a result of the occurrence of the Weddell Polynya (Fahrbach et al., 2011; Latif et al., 2013; Purkey and Johnson, 2010, 2012; Robertson et al., 2002). The Weddell Polynya, occurred as the formation of sea ice was inhibited by ocean convection and thus, transported relatively warm deep water into the surface layer (Gordon et al., 2007).

COSMOS simulations with different concentration of atmospheric CO_2 utilized in this study, have shown that external forcing plays a role in the variability of Southern Ocean SSTs. The periods of each cycle of oscillation varies from time to time for each simulation. In the same direction, the amplitude of oscillation increases with increasing CO_2. A more detailed discussion is beyond the scope of this master thesis, which is solely dedicated to the mid-Pliocene warmth.

CHAPTER 6

Conclusions and future challenges

Presented here is the layout of PlioMIP2 experiments as prescribed by Haywood et al. (2016), that have been carried out using the Earth system model COSMOS. The fully coupled atmosphere-ocean model setup consists of the atmospheric model ECHAM5, the land surface and vegetation model JSBACH, and the ocean and sea ice model MPI-OM.

The mid-Pliocene, as simulated by COSMOS and the PlioMIP2 prescribed boundary conditions is warmer than the PI-control simulation by 2.15 K in the global mean. It is also noted from this study that, the mid-Pliocene warmth are more intense in the regions where strong changes in surface albedo and orography are implemented. These regions include the Greenland and Antarctica, while the Polar warming are solely attributed to CO_2 difference between mid-Pliocene and PI simulations.
Seasonal analysis of sea ice show that mid-Pliocene Arctic ocean is sea ice free during boreal summer, with sea ice compactness dropping below 15% in most regions.

Three hypotheses were proposed and answered in this study. First is the dependence of CS on background geography. CS values for two different climate states were obtained from the COSMOS simulations with mid-Pliocene and PI geography. The CS with re-

spect to mid-Pliocene geography is 4.5 K while the corresponding value with respect to PI geography is 4.2 K per doubling of CO_2. Results obtained from this study show that CS is dependent on the background climate and on the state of the imposed boundary conditions.

The second hypothesis proposed that the agreement of simulated North Atlantic SSTs is better if the Bering Strait is closed. PlioMIP1 (with open Bering Strait) Simulation results from Stepanek and Lohmann (2012) and PlioMIP2 (with closed Bering Strait) simulations carried out in this study with the COSMOS, are compared the reconstruction of Dowsett et al. (2013). As suggested by literature, a closed Bering Strait led to a better agreement of COSMOS simulated SSTs in the North Atlantic. RMSE is used to establish simulation with the best agreement with mid-Pliocene SST reconstruction. Simulated mid-Pliocene North Atlantic SSTs show lower RMSE for PlioMIP2 than for PlioMIP1. The result is a RMSE of 2.2 for the former and the corresponding value for the latter is 2.6. Even with the closed Bering Strait, COSMOS simulated North Atlantic SSTs is still underestimated.
Hypothesis three, investigates the extent to which uncertainty in mid-Pliocene CO_2 could contribute to data-model discord. This is carried out by comparing simulations with mid-Pliocene geography and varying concentration of atmospheric CO_2. Eighteen regions of the ocean were classified and the results show that uncertainty in mid-Pliocene CO_2 contributes to the high level of data-model discrepancy.

Further steps are to be taken to improve the quality of mid-Pliocene reconstructions available for comparison with model outputs. PRISM3D reconstruction represents average climatic signals over multiple isotope excursion periods spanning from Marine Isotope Stage (MIS) G21 to M1. Therefore, prescribing present-day orbital forcing may not reproduce the expected average warm condition, as climate models are orbitally forced for a single discrete time and cannot reflect multiple changing in orbit for a continuous time interval. Haywood et al. (2013) pointed that the rampant data-model discord is highly dependent on mean annual temperature estimate based on geochemically based proxy data and is not derived from fauna-based estimates of cold-warm month means. In the

same direction, the distribution of Ocean gateways and land-sea configuration as well as atmospheric concentration of mid-Pliocene CO_2 are to be further addressed. Future mid-Pliocene studies in terms of model and data, should define new boundary conditions currently not included in the existing PRISM datasets. This might lead to a better agreement between data and model outputs.

Another interesting feature in this study, is the oscillation of COSMOS simulations with response to increasing atmospheric CO_2. This study have been able to identify the pattern of oscillation as well as the regions, where warming and cooling prevails and thus leading to the oscillation. Furthermore, it has been established that the oscillation is not only internally driven as stated by Latif et al. (2013) and external forcing play a major role triggering the oscillation.

References

Arakawa, A. and Lamb, V. R. (1977), 'Computational design of the basic dynamical processes of the UCLA general circulation model', *Methods in computational physics* **17**, 173–265.

Badger, M. P., Schmidt, D. N., Mackensen, A. and Pancost, R. D. (2013), 'High-resolution alkenone palaeobarometry indicates relatively stable pCO_2 during the Pliocene (3.3–2.8 Ma)', *Phil. Trans. R. Soc. A* **371**(2001), 20130094.

Bartoli, G., Hönisch, B. and Zeebe, R. E. (2011), 'Atmospheric CO_2 decline during the Pliocene intensification of Northern Hemisphere glaciations', *Paleoceanography* **26**(4), 4213.

Beckmann, A. and Döscher, R. (1997), 'A method for improved representation of dense water spreading over topography in geopotential-coordinate models', *Journal of Physical Oceanography* **27**(4), 581–591.

Braconnot, P., Harrison, S. P., Kageyama, M., Bartlein, P. J., Masson-Delmotte, V., Abe-Ouchi, A., Otto-Bliesner, B. and Zhao, Y. (2012), 'Evaluation of climate models using palaeoclimatic data', *Nature Climate Change* **2**(6), 417.

Brierley, C. M. and Fedorov, A. V. (2016), 'Comparing the impacts of Miocene–Pliocene

changes in inter-ocean gateways on climate: Central American seaway, Bering Strait, and Indonesia', *Earth and Planetary Science Letters* **444**, 116–130.

Brovkin, V., Raddatz, T., Reick, C. H., Claussen, M. and Gayler, V. (2009), 'Global biogeophysical interactions between forest and climate', *Geophysical Research Letters* **36**(7), 07405.

Chylek, P. and Lohmann, U. (2008), 'Aerosol radiative forcing and climate sensitivity deduced from the Last Glacial Maximum to Holocene transition', *Geophysical Research Letters* **35**(4), 04804.

Crowley, T. J. and North, G. R. (1991), 'Paleoclimatology', *International journal of Climatology* **1**, 1–339.

Dawdy, D. and Matalas, N. (1964), *Statistical and probability analysis of hydrologic data, part III: Analysis of variance, covariance and time series*, McGraw-Hill.

Dolan, A. M., Hunter, S. J., Hill, D. J., Haywood, A. M., Koenig, S. J., Otto-Bliesner, B. L., Abe-Ouchi, A., Bragg, F., Chan, W.-L., Chandler, M. A., Contoux, C., Jost, A., Kamae, Y., Lohmann, G., Lunt, D. J., Ramstein, G., Rosenbloom, N. A., Sohl, L., Stepanek, C., Ueda, H., Yan, Q. and Zhang, Z. (2015), 'Using results from the PlioMIP ensemble to investigate the Greenland Ice Sheet during the warm Pliocene', *Clim. Past* **11**, 403–424.

Dowsett, H., Dolan, A., Rowley, D., Moucha, R., Forte, A., Mitrovica, J., Pound, M., Salzmann, U., Robinson, M., Chandler, M. et al. (2016), 'The PRISM4 (mid-Piacenzian) paleoenvironmental reconstruction', *Climate of the Past* **12**(7), 1519–1538.

Dowsett, H. J., Barron, J. A., Poore, R. Z., Thompson, R. S., Cronin, T. M., Ishman, S. E. and Willard, D. A. (1999), 'Middle Pliocene paleoenvironmental reconstruction: PRISM2', *US Geological Survey open file report* **99**, 535.

Dowsett, H. J., Robinson, M. M., Stoll, D. K., Foley, K. M., Johnson, A. L., Williams, M. and Riesselman, C. R. (2013), 'The PRISM (Pliocene palaeoclimate) reconstruction: time for a paradigm shift', *Phil. Trans. R. Soc. A* **371**(2001), 20120524.

Dowsett, H., Robinson, M. and Foley, K. (2009), 'Pliocene three-dimensional global ocean temperature reconstruction', *Climate of the Past* **5**(4), 769–783.

Dowsett, H., Robinson, M., Haywood, A., Salzmann, U., Hill, D., Sohl, L., Chandler, M., Williams, M., Foley, K. and Stoll, D. (2010), 'The PRISM3D paleoenvironmental reconstruction', *Stratigraphy* **7**(2-3), 123–139.

Dowsett, H., Thompson, R., Barron, J., Cronin, T., Fleming, F., Ishman, S., Poore, R., Willard, D. and Holtz Jr, T. (1994), 'Joint investigations of the Middle Pliocene climate I: PRISM paleoenvironmental reconstructions', *Global and Planetary Change* **9**(3-4), 169–195.

Fahrbach, E., Hoppema, M., Rohardt, G., Boebel, O., Klatt, O. and Wisotzki, A. (2011), 'Warming of deep and abyssal water masses along the greenwich meridian on decadal time scales: The weddell gyre as a heat buffer', *Deep Sea Research Part II: Topical Studies in Oceanography* **58**(25), 2509–2523.

Friedrich, T., Timmermann, A., Tigchelaar, M., Timm, O. E. and Ganopolski, A. (2016), 'Nonlinear climate sensitivity and its implications for future greenhouse warming', *Science advances* **2**(11), e1501923.

Gent, P. R., Willebrand, J., McDougall, T. J. and McWilliams, J. C. (1995), 'Parameterizing eddy-induced tracer transports in ocean circulation models', *Journal of Physical Oceanography* **25**(4), 463–474.

Gladenkov, A. Y., Oleinik, A. E., Marincovich Jr, L. and Barinov, K. B. (2002), 'A refined age for the earliest opening of Bering Strait', *Palaeogeography, Palaeoclimatology, Palaeoecology* **183**(3-4), 321–328.

Gong, X., Knorr, G., Lohmann, G. and Zhang, X. (2013), 'Dependence of abrupt Atlantic meridional ocean circulation changes on climate background states', *Geophysical Research Letters* **40**(14), 3698–3704.

Gordon, A. L., Visbeck, M. and Comiso, J. C. (2007), 'A Possible Link between the Weddell Polynya and the Southern Annular Mode', *Journal of Climate* **20**(11), 2558–2571.

Hagemann, S., Dümenil, L., Maes, C., Delecluse, P. and Madec, G. (1998), 'A parametrization of the lateral waterflow for the global scale', *Climate Dynamics* **14**(1), 45–53.

Hargreaves, J. and Annan, J. (2016), 'Could the Pliocene constrain the equilibrium climate sensitivity?', *Climate of the Past* **12**(8), 1591–1599.

Haywood, A., Dowsett, H., Otto-Bliesner, B., Chandler, M., Dolan, A., Hill, D., Lunt, D., Robinson, M., Rosenbloom, N., Salzmann, U. et al. (2010), 'Pliocene model intercomparison project (PlioMIP): experimental design and boundary conditions (experiment 1)', *Geoscientific Model Development* **3**(1), 227–242.

Haywood, A., Dowsett, H., Robinson, M., Stoll, D., Dolan, A., Lunt, D., Otto-Bliesner, B. and Chandler, M. (2011), 'Pliocene Model Intercomparison Project (PlioMIP): experimental design and boundary conditions (experiment 2)', *Geoscientific Model Development* **4**(1), 571–577.

Haywood, A., Hill, D., Dolan, A., Otto-Bliesner, B., Bragg, F., Chan, W.-L., Chandler, M., Contoux, C., Dowsett, H., Jost, A. et al. (2013), 'Large-scale features of Pliocene climate: results from the Pliocene Model Intercomparison Project', *Climate of the Past* **9**(1), 191–205.

Haywood, A. M., Dowsett, H. J., Dolan, A. M., Chandler, M. A., Hunter, S. J. and Lunt, D. J. (2016), 'The Pliocene Model Intercomparison Project (PlioMIP) Phase 2: scientific objectives and experimental design', *Climate of the Past* **12**(3), 663–673.

Heydt, A., Köhler, P., Wal, R. and Dijkstra, H. A. (2014), 'On the state dependency of fast feedback processes in (paleo) climate sensitivity', *Geophysical Research Letters* **41**(18), 6484–6492.

Hibler, W. (1979), 'A dynamic thermodynamic sea ice model', *Journal of Physical Oceanography* **9**(4), 815–846.

Howell, F. W., Haywood, A. M., Otto-Bliesner, B. L., Bragg, F., Chan, W.-L., Chandler, M. A., Contoux, C., Kamae, Y., Abe-Ouchi, A., Rosenbloom, N. A., Stepanek, C. and Zhang, Z. (2016), 'Arctic sea ice in the PlioMIP ensemble', *Clim. Past* **12**, 749–767.

Hu, A., Meehl, G. A., Han, W., Otto-Bliestner, B., Abe-Ouchi, A. and Rosenbloom, N. (2015), 'Effects of the Bering Strait closure on AMOC and global climate under different background climates', *Progress in Oceanography* **132**, 174–196.

Jansen, E., Overpeck, J., Briffa, K., Duplessy, J., Joos, F., Masson-Delmotte, V., Olago, D., Otto-Bliesner, B., Peltier, W., Rahmstorf, S. et al. (2007), 'Paleoclimate', *Climate change 2007: the physical science basis; contribution of Working Group I to the Fourth Assessment Report of the Intergovernmental Panel on Climate Change* .

Jungclaus, J., Keenlyside, N., Botzet, M., Haak, H., Luo, J.-J., Latif, M., Marotzke, J., Mikolajewicz, U. and Roeckner, E. (2006), 'Ocean circulation and tropical variability in the coupled model ECHAM5/MPI-OM', *Journal of climate* **19**(16), 3952–3972.

Jungclaus, J., Lorenz, S., Timmreck, C., Reick, C., Brovkin, V., Six, K., Segschneider, J., Giorgetta, M., Crowley, T., Pongratz, J. et al. (2010), 'Climate and carbon-cycle variability over the last millennium', *Climate of the Past* **6**, 723–737.

Kageyama, M., Merkel, U., Otto-Bliesner, B., Prange, M., Abe-Ouchi, A., Lohmann, G., Ohgaito, R., Roche, D., Singarayer, J., Swingedouw, D. et al. (2013), 'Climatic impacts of fresh water hosing under Last Glacial Maximum conditions: a multi-model study', *Climate of the Past* **9**(2), 935–953.

Knorr, G., Butzin, M., Micheels, A. and Lohmann, G. (2011), 'A warm Miocene climate at low atmospheric CO_2 levels', *Geophysical Research Letters* **38**(20), 698–708.

Knutti, R., Meehl, G. A., Allen, M. R. and Stainforth, D. A. (2006), 'Constraining climate sensitivity from the seasonal cycle in surface temperature', *Journal of Climate* **19**(17), 4224–4233.

Köhler, P., Bintanja, R., Fischer, H., Joos, F., Knutti, R., Lohmann, G. and Masson-Delmotte, V. (2010), 'What caused Earth's temperature variations during the last 800,000 years? Data-based evidence on radiative forcing and constraints on climate sensitivity', *Quaternary Science Reviews* **29**(1-2), 129–145.

Latif, M., Martin, T. and Park, W. (2013), 'Southern Ocean Sector Centennial Climate Variability and Recent Decadal Trends', *Journal of Climate* **26**(19), 7767–7782.

Legutke, S. and Maier-Reimer, E. (2002), 'The impact of a downslope water-transport parametrization in a global ocean general circulation model', *Climate dynamics* **18**(7), 611–623.

Lin, S.-J. and Rood, R. B. (1996), 'Multidimensional Flux-Form semi-Lagrangian transport schemes', *Monthly Weather Review* **124**(9), 2046–2070.

Lisiecki, L. E. and Raymo, M. E. (2005), 'A Pliocene-Pleistocene stack of 57 globally distributed benthic δ180 records', *Paleoceanography* **20**(1), 1–17.

Lohmann, G. (1998), 'The influence of a near-bottom transport parameterization on the sensitivity of the thermohaline circulation', *Journal of Physical Oceanography* **28**(10), 2095–2103.

Lohmann, G., Newman, L. and Kiefer, T. (2008), 'Data-model comparison', *PAGES News* **16**(2), 1–40.

Lohmann, G., Pfeiffer, M., Laepple, T., Leduc, G. and Kim, J.-H. (2013), 'A model-data comparison of the Holocene global sea surface temperature evolution', *Climate of the Past* (9), 1807–1839.

Lott, F. (1999), 'Alleviation of stationary biases in a GCM through a mountain drag parameterization scheme and a simple representation of mountain lift forces', *Monthly weather review* **127**(5), 788–801.

Lott, F. and Miller, M. J. (1997), 'A new Subgrid-scale orographic drag parametrization: Its formulation and testing', *Quarterly Journal of the Royal Meteorological Society* **123**(537), 101–127.

Lunt, D. J., Haywood, A. M., Schmidt, G. A., Salzmann, U., Valdes, P. J. and Dowsett, H. J. (2010), 'Earth system sensitivity inferred from Pliocene modelling and data', *Nature Geoscience* **3**(1), 60–74.

Marsland, S. J., Haak, H., Jungclaus, J. H., Latif, M. and Röske, F. (2003), 'The Max-Planck-Institute global ocean/sea ice model with orthogonal curvilinear coordinates', *Ocean modelling* **5**(2), 91–127.

Motoi, T., Chan, W.-L., Minobe, S. and Sumata, H. (n.d.), 'North Pacific halocline and cold climate induced by Panamanian Gateway closure in a coupled ocean-atmosphere GCM', *Geophysical Research Letters* **32**(10), 1–4.

Myhre, G., Highwood, E. J., Shine, K. P. and Stordal, F. (1998), 'New estimates of radiative forcing due to well mixed greenhouse gases', *Geophysical Research Letters* **25**(14), 2715–2718.

Otto-Bliesner, B. L., Brady, E. C., Fasullo, J., Jahn, A., Landrum, L., Stevenson, S., Rosenbloom, N., Mai, A. and Strand, G. (2016), 'Climate variability and change since 850 CE: an ensemble approach with the community earth system model', *Bulletin of the American Meteorological Society* **97**(5), 735–754.

Otto-Bliesner, B. L., Jahn, A., Feng, R., Brady, E. C., Hu, A. and Löfverström, M. (2017), 'Amplified North Atlantic warming in the late Pliocene by changes in Arctic gateways', *Geophysical Research Letters* **44**(2), 957–964.

Pagani, M., Liu, Z., LaRiviere, J. and Ravelo, A. C. (2010), 'High Earth-system climate sensitivity determined from Pliocene carbon dioxide concentrations', *Nature Geoscience* **3**(1), 27–41.

Pound, M., Tindall, J., Pickering, S., Haywood, A., Dowsett, H. and Salzmann, U. (2014), 'Late Pliocene lakes and soils: a global data set for the analysis of climate feedbacks in a warmer world', *Climate of the Past* **10**(1), 167–180.

Purkey, S. G. and Johnson, G. C. (2010), 'Warming of global abyssal and deep Southern Ocean waters between the 1990s and 2000s: Contributions to global heat and sea level rise budgets', *Journal of Climate* **23**(23), 6336–6351.

Purkey, S. G. and Johnson, G. C. (2012), 'Global contraction of Antarctic Bottom Water between the 1980s and 2000s', *Journal of Climate* **25**(17), 5830–5844.

Raddatz, T., Reick, C., Knorr, W., Kattge, J., Roeckner, E., Schnur, R., Schnitzler, K.-G., Wetzel, P. and Jungclaus, J. (2007), 'Will the tropical land biosphere dominate the climate–carbon cycle feedback during the twenty-first century?', *Climate Dynamics* **29**(6), 565–574.

Raymo, M. E., Mitrovica, J. X., OLeary, M. J., DeConto, R. M. and Hearty, P. J. (2011), 'Departures from eustasy in Pliocene sea-level records', *Nature Geoscience* **4**(5), 328–340.

Raymo, M., Grant, B., Horowitz, M. and Rau, G. (1996), 'Mid-Pliocene warmth: stronger greenhouse and stronger conveyor', *Marine Micropaleontology* **27**(1), 313 – 326.

Robert, A. (1981), 'A stable numerical integration scheme for the primitive meteorological equations', *Atmosphere-Ocean* **19**(1), 35–46.

Robert, A. (1982), 'A semi-lagrangian and semi-implicit numerical integration scheme for the primitive meteorological equations', *Journal of the Meteorological Society of Japan. Ser. II* **60**(1), 319–325.

Robert, A., Henderson, J. and Turnbull, C. (1972), 'An implicit time integration scheme for baroclinic models of the atmosphere', *Monthly Weather Review* **100**(5), 329–335.

Robertson, R., Visbeck, M., Gordon, A. L. and Fahrbach, E. (2002), 'Long-term temperature trends in the deep waters of the Weddell Sea', *Deep Sea Research Part II: Topical Studies in Oceanography* **49**(21), 4791–4806.

Robinson, M. M. (2009), 'New quantitative evidence of extreme warmth in the Pliocene Arctic', *Stratigraphy* **6**(4), 265–277.

Robinson, M. M., Valdes, P. J., Haywood, A. M., Dowsett, H. J., Hill, D. J. and Jones, S. M. (2011), 'Bathymetric controls on Pliocene North Atlantic and Arctic sea surface temperature and deepwater production', *Palaeogeography, Palaeoclimatology, Palaeoecology* **309**(1-2), 92–97.

Roeckner, E., Bäuml, G., Bonaventura, L., Brokopf, R., Esch, M., Giorgetta, M., Hagemann, S., Kirchner, I., Kornblueh, L., Manzini, E. et al. (2003), 'The atmospheric general circulation model ECHAM 5. PART I: Model description', **349**, 1–140.

Rohling, E., Sluijs, A., Dijkstra, H., Köhler, P., Van de Wal, R., Von Der Heydt, A., Beerling, D., Berger, A., Bijl, P., Crucifix, M. et al. (2012), 'Making sense of palaeoclimate sensitivity', *Nature* **491**(7426), 683–691.

Rowley, D. B., Forte, A. M., Moucha, R., Mitrovica, J. X., Simmons, N. A. and Grand, S. P. (2013), 'Dynamic topography change of the eastern united states since 3 million years ago', *Science* **340**(6140), 1560–1563.

Salzmann, U., Dolan, A. M., Haywood, A. M., Chan, W.-L., Voss, J., Hill, D. J., Abe-Ouchi, A., Otto-Bliesner, B., Bragg, F. J., Chandler, M. A. et al. (2013), 'Challenges in quantifying Pliocene terrestrial warming revealed by data–model discord', *Nature Climate Change* **3**(11), 969–974.

Salzmann, U., Haywood, A., Lunt, D., Valdes, P. and Hill, D. (2008), 'A new global biome reconstruction and data-model comparison for the middle Pliocene', *Global Ecology and Biogeography* **17**(3), 432–447.

Sewall, J. O., Van de Wal, R., Van Der Zwan, K., Van Oosterhout, C., Dijkstra, H. and Scotese, C. (2007), 'Climate model boundary conditions for four Cretaceous time slices', *Climate of the Past* **3**(4), 647–657.

Sohl, L. E., Chandler, M. A., Schmunk, R. B., Mankoff, K., Jonas, J. A., Foley, K. M. and Dowsett, H. J. (2009), PRISM3/GISS topographic reconstruction, Technical report, US Geological Survey.

Stepanek, C. and Lohmann, G. (2012), 'Modelling mid-Pliocene climate with COSMOS', *Geoscientific Model Development* **5**(5), 1221–1243.

Varma, V., Prange, M., Merkel, U., Kleinen, T., Lohmann, G., Pfeiffer, M., Renssen, H., Wagner, A., Wagner, S. and Schulz, M. (2012), 'Holocene evolution of the Southern Hemisphere westerly winds in transient simulations with global climate models', *Climate of the Past* **8**, 391–402.

von der Heydt, A. S. and Ashwin, P. (2016), 'State dependence of climate sensitivity: attractor constraints and palaeoclimate regimes', *Dynamics and Statistics of the Climate System* **1**(1), 001–015.

Walker, G. (2010), *An Ocean of Air: A Natural History of the Atmosphere*, Bloomsbury Publishing.

Walker, J., Geissman, J., Bowring, S. and Babcock, L. (2013), 'The geological society of america geologic time scale', *GSA Bulletin* **125**(3-4), 1–259.

Wei, W. and Lohmann, G. (2012), 'Simulated Atlantic Multidecadal Oscillation during the Holocene', *Journal of Climate* **25**(20), 6989–7002.

Yoshimori, M., Hargreaves, J. C., Annan, J. D., Yokohata, T. and Abe-Ouchi, A. (2011), 'Dependency of feedbacks on forcing and climate state in physics parameter ensembles', *Journal of Climate* **24**(24), 6440–6455.

Zhang, Z.-S., Nisancioglu, K. H., Chandler, M. A., Haywood, A. M., Otto-Bliesner, B. L., Ramstein, G., Stepanek, C., Abe-Ouchi, A., Chan, W.-L., Bragg, F. J. et al. (2013), 'Mid-Pliocene Atlantic meridional overturning circulation not unlike modern', *Climate of the Past* **9**, 1495–1504.